nature communications

Article

https://doi.org/10.1038/s41467-025-59591-8

Impaired ketogenesis in Leydig Cells drives testicular aging

Received: 23 July 2024

Accepted: 17 April 2025

Published online: 07 May 2025

Check for updates

Congyuan Liu[1,2,8], Hao Peng[1,2,8], Jiajie Yu[3,8], Peng Luo[4,8], Chuanfeng Xiong[1,2], Hong Chen[5,6], Hang Fan[1,2], Yuanchen Ma[1,2], Wangsheng Ou[7], Suyuan Zhang[1,2], Cuifeng Yang[3], Lerong Zhao[1,2], Yuchen Zhang[1,2], Xiaolu Guo[5,6], Qiong Ke[1,2], Tao Wang[1,2], Chunhua Deng[3], Weiqiang Li[1,2], Andy Peng Xiang[1,2] ✉ & Kai Xia[1,2] ✉

Testicular aging commonly leads to testosterone deficiency and impaired spermatogenesis, yet the underlying mechanisms remain elusive. Here, we show that Leydig cells are particularly vulnerable to aging processes in testis. Single-cell RNA sequencing identifies the expression of *Hmgcs2*, the gene encoding rate-limiting enzyme of ketogenesis, decreases significantly in Leydig cells from aged mice. Additionally, the concentrations of ketone bodies β-hydroxybutyric acid and acetoacetic acid in young testes are substantially higher than that in serum, but significantly diminish in aged testes. Silencing of *Hmgcs2* in young Leydig cells drives cell senescence and accelerated testicular aging. Mechanistically, β-hydroxybutyric acid upregulates the expression of *Foxo3a* by facilitating histone acetylation, thereby mitigating Leydig cells senescence and promoting testosterone production. Consistently, enhanced ketogenesis by genetic manipulation or oral β-hydroxybutyric acid supplementation alleviates Leydig cells senescence and ameliorates testicular aging in aged mice. These findings highlight defective ketogenesis as a pivotal factor in testicular aging, suggesting potential therapeutic avenues for addressing age-related testicular dysfunction.

The testis is fundamental to male reproductive health, playing a pivotal role in both spermatogenesis and the synthesis of male sex hormones throughout an individual's life[1,2]. As men age, a progressive decline in spermatogenesis significantly contributes to male infertility and increases the risk of genetic and other abnormalities in their progeny[3,4]. Additionally, testicular aging is also characterized by a reduction in testosterone, which is linked to various male reproductive disorders and a diminished quality of life in the elderly[5]. Currently, testosterone replacement therapy (TRT) serves as the primary intervention for alleviating symptoms associated with testicular aging[6]. However, TRT is accompanied by notable adverse effects, including an elevated risk of cardiovascular

[1]Center for Stem Cell Biology and Tissue Engineering, Key Laboratory for Stem Cells and Tissue Engineering, Ministry of Education, Sun Yat-sen University, Guangzhou, Guangdong, China. [2]National-Local Joint Engineering Research Center for Stem Cells and Regenerative Medicine, Zhongshan School of Medicine, Sun Yat-sen University, Guangzhou, Guangdong, China. [3]Department of Urology and Andrology, The First Affiliated Hospital, Sun Yat-sen University, Guangzhou, Guangdong, China. [4]Reproductive Medicine Center, The First Affiliated Hospital, Sun Yat-sen University, The Key Laboratory for Reproductive Medicine of Guangdong Province, Guangzhou, Guangdong, China. [5]Center for Stem Cells Translational Medicine, Shenzhen Qianhai Shekou Free Trade Zone Hospital, Shenzhen, Guangdong, China. [6]Brain Cognition and Brain Disease Institute, Shenzhen Institutes of Advanced Technology, Chinese Academy of Sciences, Shenzhen, Guangdong, China. [7]State Key Laboratory of Ophthalmology, Zhong Shan Ophthalmic Center, Sun Yat-sen University, Guangzhou, Guangdong, China. [8]These authors contributed equally: Congyuan Liu, Hao Peng, Jiajie Yu, Peng Luo. ✉e-mail: xiangp@mail.sysu.edu.cn; xiak7@mail.sysu.edu.cn

diseases, exacerbation of sleep apnea syndrome, and an increased possibility of developing prostate cancer[7,8]. Moreover, TRT fails to mimic the physiological secretion patterns of testosterone and can negatively impact spermatogenesis[9,10]. Consequently, there is a pressing need to explore novel therapeutic strategies for addressing testicular aging.

Cellular senescence has been classically described as a stable cell cycle arrest that develops in response to stress or damage, thereby triggering multiple intracellular phenotypic changes[11]. Senescent cells are characterized by features such as enlarged cell size, DNA damage, and the secretion of senescence-associated secretory phenotype (SASP) factors[11,12]. Notably, senescent cells accumulate in vivo with aging and are associated with disrupted tissue homeostasis and diminished regenerative capacity[13]. Recent evidence has implicated accumulation of senescent cells as a contributing factor to aging and age-related diseases in fast-aging and naturally aged mice models. For instance, the transplantation of a small number of senescent cells around the knee joint was sufficient to induce osteoarthritis[14]. In addition, transplanting senescent ear fibroblasts or syngeneic pre-adipocytes into middle-aged mice can induce frailty, accelerate the onset of all age-related diseases, and lead to premature death when compared to transplanting equivalent numbers of non-senescent cells[15]. Conversely, recent studies have showed that alleviating cellular senescence could effectively delay organ aging and address aging-related diseases. In muscle, inhibiting 15-PGDH (15-hydroxyprostaglandin dehydrogenase) in senescent myofibers could enhance aged muscle mass, strength, and exercise performance[16]. In blood vessels, knockout of GIGYF2(Grb10-interacting GYF protein 2) in senescent vascular endothelial cells could protect aged mice from aging-associated vascular endothelium-dependent relaxation and arterial stiffness[17]. Therefore, targeting senescent cells presents a promising pathway for developing novel and effective anti-aging therapeutics.

Aging testes undergo profound alterations in both germ cells and somatic cells, leading to reduced functionality[18,19]. Previous studies have shown that testicular aging is marked by a decline in the number of spermatogonia and spermatocytes, as well as the accumulation of DNA damage and mutations within germline cells[4,20]. As the primary cells producing testosterone, LCs play a crucial role in spermatogenesis and male fertility[21]. LCs are thought to be vulnerable to age-related damage, primarily due to oxidative stress induced by reactive oxygen species (ROS). This susceptibility can contribute to the development of late-onset hypogonadism[22,23]. An alternative view suggests that Sertoli cells are also susceptible to aging, since Sertoli cells expressed senescent markers in the aged testes[24]. A recent study reported that compromised lysosomal acidity in aged Sertoli cells disrupts autophagy and phagocytic flow, leading to testicular aging[25]. Nevertheless, a systematic profiling of senescent cells in the testes during aging has yet to be established.

In this study, we characterize testicular aging by detecting the senescence marker senescence-associated β-galactosidase (SA-β-gal), identifying that LCs are the most susceptible cells to aging in the testis. Single-cell transcriptomics reveals a significant down-regulation of 3-Hydroxy-3-methylglutaryl-CoA synthase 2 (*Hmgcs2*), which encodes the rate-limiting enzyme in ketogenesis, in aged LCs. Moreover, silence of *Hmgcs2* in young LCs impairs ketogenesis, causing premature senescence and accelerating testicular aging. Mechanistically, β-hydroxybutyric acid (BHB), a ketogenic product and inhibitor of histone deacetylase 1 (HDAC1), promotes *Foxo3a* expression by enhancing histone acetylation, thereby alleviating LCs senescence and improving steroidogenic function. In vivo studies further demonstrate that enhancing ketogenesis via *Hmgcs2* overexpression or BHB supplementation reduces LCs senescence and improves testicular function in aged mice.

Results

LCs are susceptible to senescence during the process of aging in mice

To investigate the phenotypic changes and underlying mechanisms of testicular aging, testes were harvested from young (2-month-old) and aged (24-month-old) mice. Morphological analysis revealed a reduction in the diameter of seminiferous tubules and the thickness of the seminiferous epithelium in aged mice (Supplementary Fig. 1a–c). Consistently, sperm analysis demonstrated a significant decrease in sperm concentration and motility in the aged group (Supplementary Fig. 1d–g). Subsequently, we analyzed the levels of sex hormones in the aged group. Testosterone assays revealed that serum and intratesticular testosterone levels decreased significantly in aged mice (Supplementary Fig. 1h, i). In addition, Insulin-like peptide 3 (Insl3), indicative of LCs function, was reduced in the aged group (Supplementary Fig. 1j). Since testosterone levels are regulated by gonadotropins, we measured the concentrations of luteinizing hormone (LH) and follicle-stimulating hormone (FSH) levels in both groups. As expected, LH and FSH levels were elevated in the aged group (Supplementary Fig. 1k, l). Collectively, these histological and functional analysis revealed significant testicular aging in aged mice.

The accumulation of senescent cells is a driving force in physical functional decline in various tissues during aging[26]. To further quantify cellular senescence in the testis, we performed SA-β-gal staining on the testes of 2-, 8-, 16-, and 24-month-old mice. Surprisingly, we observed a notable increase in SA-β-gal$^+$ cells appeared as early as 8 months of age and SA-β-gal$^+$ signals were specifically located in the interstitium of testes during aging, indicating that interstitial cells are more susceptible to aging than Sertoli cells and germ cells (Supplementary Fig. 1m). The specific cell types from testes were further analyzed by co-immunostaining with SA-β-gal and previously described cell markers. The results revealed that SA-β-gal$^+$ cells largely co-expressed with the LCs marker CYP17A1 (Supplementary Fig. 1n, o). However, macrophages and Sertoli cells did not show SA-β-gal staining on testes of 8-month-old mice (Supplementary Fig. 1p). These results underscore that LCs are highly vulnerable to aging.

Single-cell transcriptomic profile of testicular aging reveals a senescence signature of LCs

To investigate the molecular changes associated with LCs senescence, testicular cells were isolated from 3 young mice (2-month-old) and 3 aged mice (24-month-old), followed by single-cell RNA sequencing (scRNA-seq) using the BD Rhapsody platform (Fig. 1a). Data from 2584 and 4344 cells passed quality control (Supplementary Fig. 2a, b) and were included in the subsequent analysis for young and aged samples, respectively (Fig. 1a). Using unbiased clustering and t-Distributed Stochastic Neighbor Embedding (tSNE) analysis, we identified the following 7 cell types based on the expression of specific marker genes: LCs (*Cyp17a1*, *Star*, *Lhcgr*), mesenchymal cells (MCs; *Pdgfrα*, *Arx*, *Tcf21*), macrophages (Ms; *Adgre1*, *Mrc1*, *Itgam*), spermatogonia (SPGs; *Id4*, *Tspan33*, *Dazl*), spermatocytes (SPCs; *Sycp3*, *Zpbp2*, *Pgk2*), round spermatids (RSs; *Acrv1*, *Spag6*, *Tssk1*), and elongating spermatids (ESs; *Prm1*, *Tnp2*, *Prm3*) (Fig. 1b, c; Supplementary Fig. 2c). Analysis of the top 30 marker genes revealed that each cell type had unique transcriptional features and enriched pathways relevant to their distinct biological functions (Fig. 1d).

We next performed a focused analysis of age-associated changes in the LCs cluster. Not surprisingly, clustering analysis revealed that LCs from young and aged mice exhibited two distinct subpopulations (Fig. 1e). Furthermore, we examined the expression of senescence-related markers and found that *p21* (known as Cyclin-dependent kinase inhibitor 1 A, *Cdkn1a*) and *Cxcl10* exhibited transcriptional upregulation in LCs obtained from the aged testes compared to the young group (Fig. 1e). To validate the gene expression pattern, we performed quantitative RT-PCR analysis, revealing significantly increased

https://doi.org/10.1038/s41467-025-59591-8

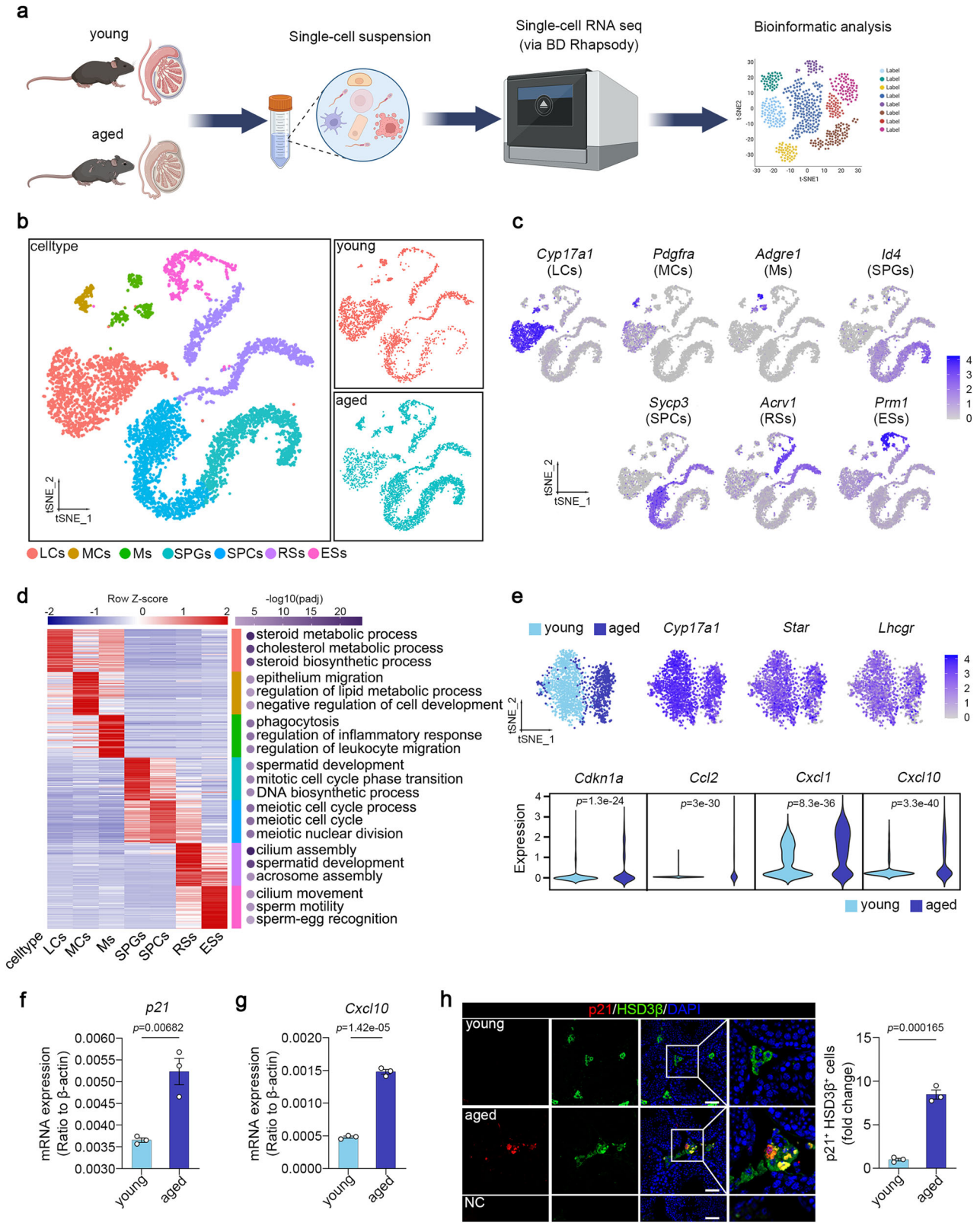

expression of *p21* and *Cxcl10* in the aged group (Fig. 1f, g). Consistently, immunostaining analysis confirmed that the protein levels of p21 showed a substantial increase in LCs from the aged group compared to the young group (Fig. 1h). These findings collectively indicate that testicular aging is accompanied by the accumulation of senescent LCs, which may lead to morphological changes and functional impairment.

Senescent LCs of aged mice exhibit impaired ketogenesis

To further characterize the ageing-associated changes of gene expression in LCs during testicular aging, we performed gene set enrichment analysis (GSEA) based on gene ontology (GO) database. Our results revealed that the genes upregulated with age were mainly associated with response to inflammation-related terms, such as "cellular response to interleukin 1" and "positive regulation of alpha beta t

Fig. 1 | Single-cell transcriptome profiling of young and aged mice testes. **a** Schematic of the experimental workflow. **b** Left: tSNE (t-Distributed Stochastic Neighbor Embedding) plot showing the annotated testicular cell types of mice testes. Cells are colored and annotated by cell types. Right: tSNE plots showing distribution of different cell types in the young (top) and aged (bottom) testes. **c** tSNE plot showing the expression profiles of the indicated cell type-specific marker genes for the assessed cell types in mice testes. The color key, ranging from grey to blue, indicates low to high gene expression levels, respectively. **d** Left: heatmap showing the top 30 differentially expressed genes of each cell cluster. The scaled gene expression levels were colored according to Z-score at the top. Right: the corresponding GO terms enriched in each cell cluster with -log10 (adjusted *P*-value) colored according to the color key at the top. **e** tSNE plot showing young and aged LCs populations. Violin plots showing the expression of senescence markers in young and aged LCs. **f, g** Quantitative RT-PCR analysis of senescence markers (*p21*, *Cxcl10*) in LCs from young and aged mice. $n = 3$ per group. **h** Left: representative confocal images of testicular sections obtained from young and aged mice. NC: negative control. The sections were stained with senescence marker p21 (Cyclin-dependent kinase inhibitor 1 A), HSD3β (hydroxysteroid dehydrogenase-3β), and DAPI (4,6-diamino-2-phenyl indole). Right: quantitative analysis of the $p21^+$ $HSD3\beta^+$ cells. Scale bar: 50 μm. $n = 3$ per group. Data were presented as mean ± SEM. Significance was determined by Two-tailed t-test (**f**–**h**), or Two-sided Wilcoxon rank-sum test (**e**) or One-sided hypergeometric test with BH correction (**d**). Illustrations were created in BioRender. Xia, K. (2025) https://BioRender.com/2y29pus. Source data are provided as a Source Data file.

cell activation". By comparison, the downregulated DEGs were enriched in metabolism-related terms, including "aerobic respiration", "generation of precursor metabolites and energy", and "cholesterol catabolic process" (Fig. 2a). To identify critical regulators linked to LCs aging, we analyzed aging-associated differentially expressed genes (DEGs) based on the above GO terms. Among these DEGs, *Hmgcs2* exhibited the most prominent changes, with notable downregulation in LCs from the aged group (Fig. 2b). *Hmgcs2* is the gene encoding the rate-limiting enzyme for ketogenesis[27,28] (Fig. 2c). Therefore, we examined the expression of genes encoding other ketogenic enzymes, including acetyl-CoA acetyltransferase 1 (*Acat1*), Hmg-CoA lyase (*Hmgcl*) and 3-hydroxybutyrate dehydrogenase 1 (*Bdh1*)[27]. The analysis of scRNA-seq data revealed downregulation of *Hmgcl* in aged LCs, however, *Bdh1* and *Acat* showed no significant difference between young and aged LCs (Fig. 2d). To validate these findings, we isolated primary LCs from the young and aged testes and assessed genes expression using quantitative RT-PCR. The results demonstrated a substantial decrease in the expression of ketogenesis-related enzymes, including *Acat*, *Hmgcs2*, and *Hmgcl* in aged mice (Fig. 2e–g). Additionally, immunofluorescence staining revealed a significant reduction in HMGCS2 expression in LCs from aged mice (Fig. 2h). The primary ketone bodies include acetoacetic acid (AcAc) and its redox partner β-hydroxybutyric acid (BHB)[28]. To assess ketogenesis levels in the testis, we measured intratesticular ketone body concentrations. As expected, BHB and AcAc concentrations showed significant decreases in the aged testes compared to the young testes (Fig. 2i, j). However, BHB and AcAc concentrations in serum were comparable between the young and the aged group (Fig. 2k, l). Remarkably, the concentration of ketone bodies in the testes were more than tenfold higher than that in serum (Fig. 2i–l), implying ketone bodies might have testis-specific functions. In summary, these results indicate that ketogenesis is impaired in the LCs of aged testis.

Suppression of ketogenesis induces senescence of LCs in vitro

Next, we investigated whether impaired ketogenesis induces premature senescence of LCs. For this purpose, MLTC-1 cells (cell line of LCs) were treated with an HMGCS2 inhibitor Hymeglusin (3 μM) for 4 days in culture (Fig. 3a). As evidenced by the reduced levels of ketone bodies in MLTC-1 cells, Hymeglusin treatment effectively inhibited ketogenesis (Fig. 3b, c). After Hymeglusin treatment, an increase in SA-β-gal^+ cells was observed (Fig. 3d), along with increased immunofluorescent staining for the senescence marker γ-H2AX and H2AY, as well as reduced Lamin B expression (Fig. 3e–g). Quantitative RT-PCR analysis revealed a significant upregulation of senescence markers *p21* and Plasminogen activator inhibitor-1 (*Pai1*) in Hymeglusin treated MLTC-1 cells (Fig. 3h, i). Additionally, Hymeglusin treatment resulted in a significant decrease in progesterone level in the culture medium of MLTC-1 cells, indicating suppression of ketogenesis impairs steroidogenic function of LCs (Fig. 3j). To confirm these findings, we performed bulk RNA-seq on MLTC-1 cells treated with Hymeglusin or vehicle. The results revealed marked alterations in global gene expression following Hymeglusin treatment (Fig. 3k). Notably, these changes closely resembled those observed during natural aging. Specifically, DEGs upregulated by Hymeglusin were primarily associated with inflammation and cell cycle arrest, such as terms involved in "negative regulation of cell cycle phase transition" and "innate immune response". In contrast, downregulated DEGs were enriched in metabolism-related pathways, including "generation of precursor metabolites and energy", "fatty acid metabolic process", and "cholesterol metabolic process" (Fig. 3l). These findings suggest that impaired ketogenesis leads to the appearance of aging phenotype in LCs.

To specifically investigate the effects of *Hmgcs2* on senescence, we further used a genetic approach to reduce enzyme levels in MLTC-1 cells by introducing either shRNA to *Hmgcs2* or a scrambled (scr) shRNA under the control of a ubiquitous promoter CAG through lentivirus. The knockdown efficiency of *Hmgcs2* was confirmed by Western blot analysis, and a reduction in ketone bodies levels was observed in MLTC-1 cells 7 days after transfection (Supplementary Fig. 3a–c). Similarly, knockdown of *Hmgcs2* increased the number of SA-β-gal^+ cells and enhanced expression of γ-H2AX, H2AY, as well as reduced expression of Lamin B in MLTC-1 cells (Supplementary Fig. 3d–g). Quantitative RT-PCR also revealed significant upregulation of *p21* and *Pai1* expression in the *Hmgcs2*-knockdown cells (Supplementary Fig. 3h, i). Furthermore, knockdown of *Hmgcs2* significantly suppressed progesterone production compared to the control group (Supplementary Fig. 3j). Collectively, these findings suggest that impaired ketogenesis drives the senescence of LCs.

Knockout of *Hmgcs2* drives LCs senescence and testicular aging in young mice

To further elucidate the effect of ketogenesis on LCs senescence in vivo, we generated a *Hmgcs2-flox* ($Hmgcs2^{fl/fl}$) mouse line on C57BL/6 background. Recent studies have indicated that adeno-associated virus (AAV) vectors exhibit tropism for LCs when injected into testes[29,30]. We therefore interstitially injected AAV serotype DJ encoding GFP under the control of the CAG promoter (AAV-GFP) at titers of 2×10^9 genome copies (gc) into each testis of 8-week-old wild type mice. Seven days post-injection, immunofluorescence analysis revealed that GFP was expressed exclusively in the interstitium of testis, with no off-target transduction detected in the liver, kidney, heart, brain, lung, intestine, or muscle (Supplementary Fig. 4a). Moreover, GFP expression was specific to $CYP17A1^+$ cells in the injected testes, confirming that AAV specifically target LCs when delivered into the interstitial compartment (Supplementary Fig. 4b). Next, 8-week-old $Hmgcs2^{fl/fl}$ mice were subjected to intratesticular injections of AAV-GFP or AAV-Cre at titers of 2×10^9 genome copies (gc) into each testis (Fig. 4a). Four weeks after injection, quantitative RT-PCR analysis of testicular tissue showed a significant decline in *Hmgcs2* transcripts (Supplementary Fig. 4c), and Western blot assays demonstrated a corresponding decrease in HMGCS2 protein levels in AAV-Cre group compared with AAV-GFP group (Supplementary Fig. 4d). Immunofluorescence staining also confirmed a reduction of HMGCS2 in LCs from AAV-Cre group (Fig. 4b). Moreover, the concentrations of

https://doi.org/10.1038/s41467-025-59591-8

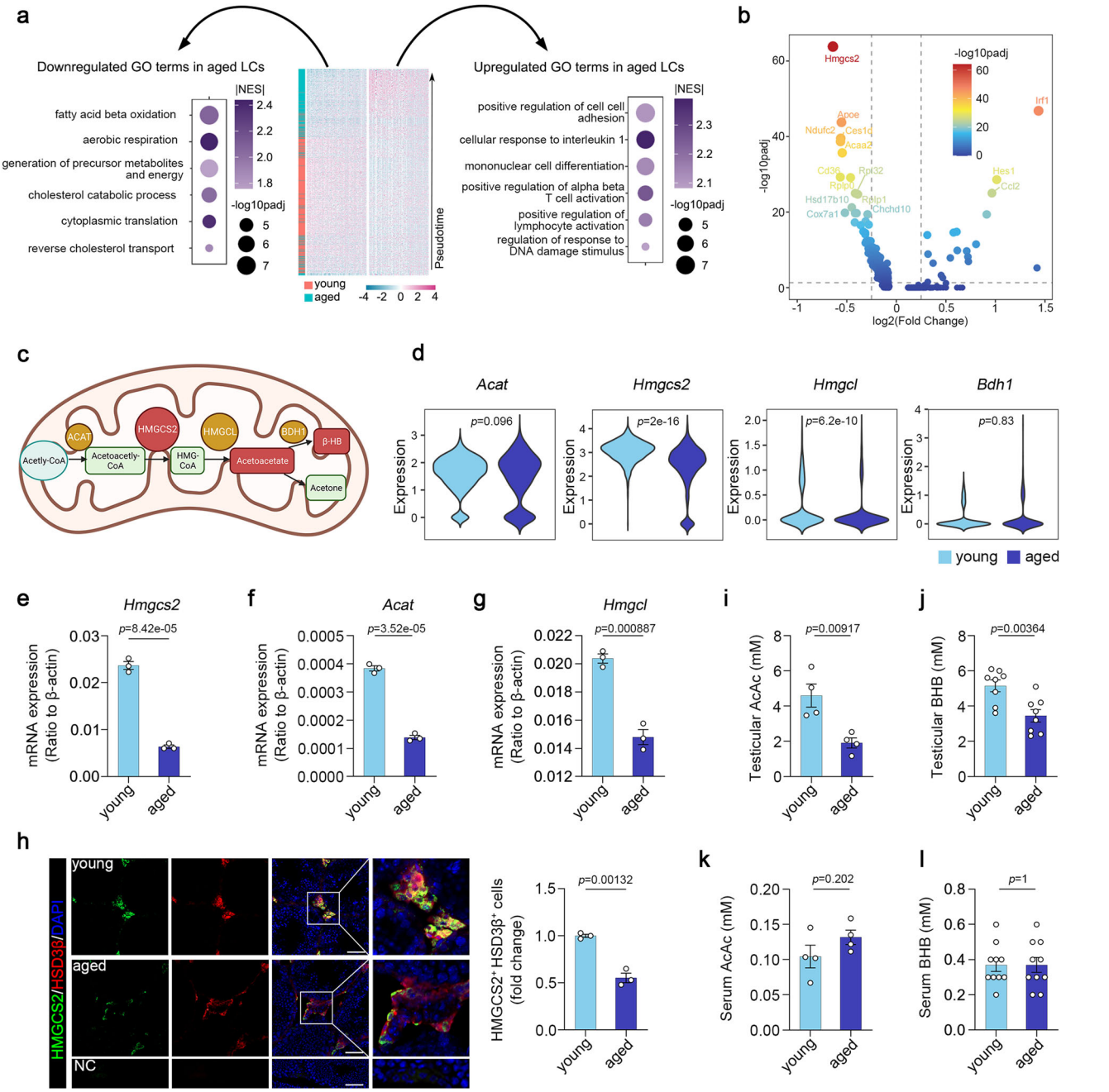

Fig. 2 | LCs in the aged testis show impaired ketogenesis, which leads to a decrease in testicular ketone body concentration. a Heatmap showing both the upregulated and downregulated DEGs in the aged group of LCs. The scaled gene expression levels are colored according to Z-score. Six upregulated or downregulated GO terms of DEGs were listed, with dot size indicating the range of −log10 (adjusted *P*-value). Color keys, ranging from grey to blue, indicate the absolute value of the NES. **b** Volcano plots of the upregulated and downregulated genes in GO terms listed in (**a**). **c** Diagram of ketogenesis. **d** Violin plots showing the expression of genes encoding enzymes for ketogenesis in LCs. **e**–**g** Quantitative RT-PCR analysis of genes encoding enzymes for ketogenesis in primary LCs. $n = 3$ per group. **h** Left: representative confocal images of testicular sections obtained from young and aged mice. NC: negative control. The sections were stained with HMGCS2 (3-hydroxy-3-methylglutaryl-CoA synthetase 2), HSD3β, and DAPI. Scale bar: 50 μm. Right: quantitative analysis of the $HMGCS2^+$ $HSD3\beta^+$ cells. $n = 3$ per group. **i**–**l** The concentration of ketone bodies in serum or testes. $n = 4$ per group in (**i**) and (**k**); $n = 8$ per group in (**j**), $n = 10$ per group in (**l**). Data were presented as mean ± SEM. Significance was determined by Two-tailed t-test (**e**–**l**), or Two-sided Wilcoxon rank-sum test with bonferroni correction (**b, d**) or Two-sided permutation test with BH correction (**a**). Illustrations were created with BioRender. Source data are provided as a Source Data file.

testicular BHB and AcAc showed significant decline in AAV-Cre treated mice (Fig. 4c, d; Supplementary Fig. 4e, f).

To determine whether the conditional knockout of *Hmgcs2* induces LCs senescence, we performed SA-β-gal staining on the testes 2 months post-injection. The number of SA-β-gal$^+$ LCs increased significantly in the testes from AAV-Cre treated group (Fig. 4e). Immunofluorescence analysis also revealed a significant increase in the senescence marker p21 in LCs from AAV-Cre treated group (Fig. 4f). Quantitative RT-PCR of isolated LCs showed significant upregulation of senescence markers *p21* and *Cxcl10* in AAV-Cre treated group compared to AAV-GFP treated group (Fig. 4g, h). Additionally, serum and intratesticular testosterone concentrations decreased significantly in AAV-Cre treated mice compared to AAV-GFP treated mice (Fig. 4i, j). Similarly, serum Insl3 concentrations were significantly reduced

https://doi.org/10.1038/s41467-025-59591-8

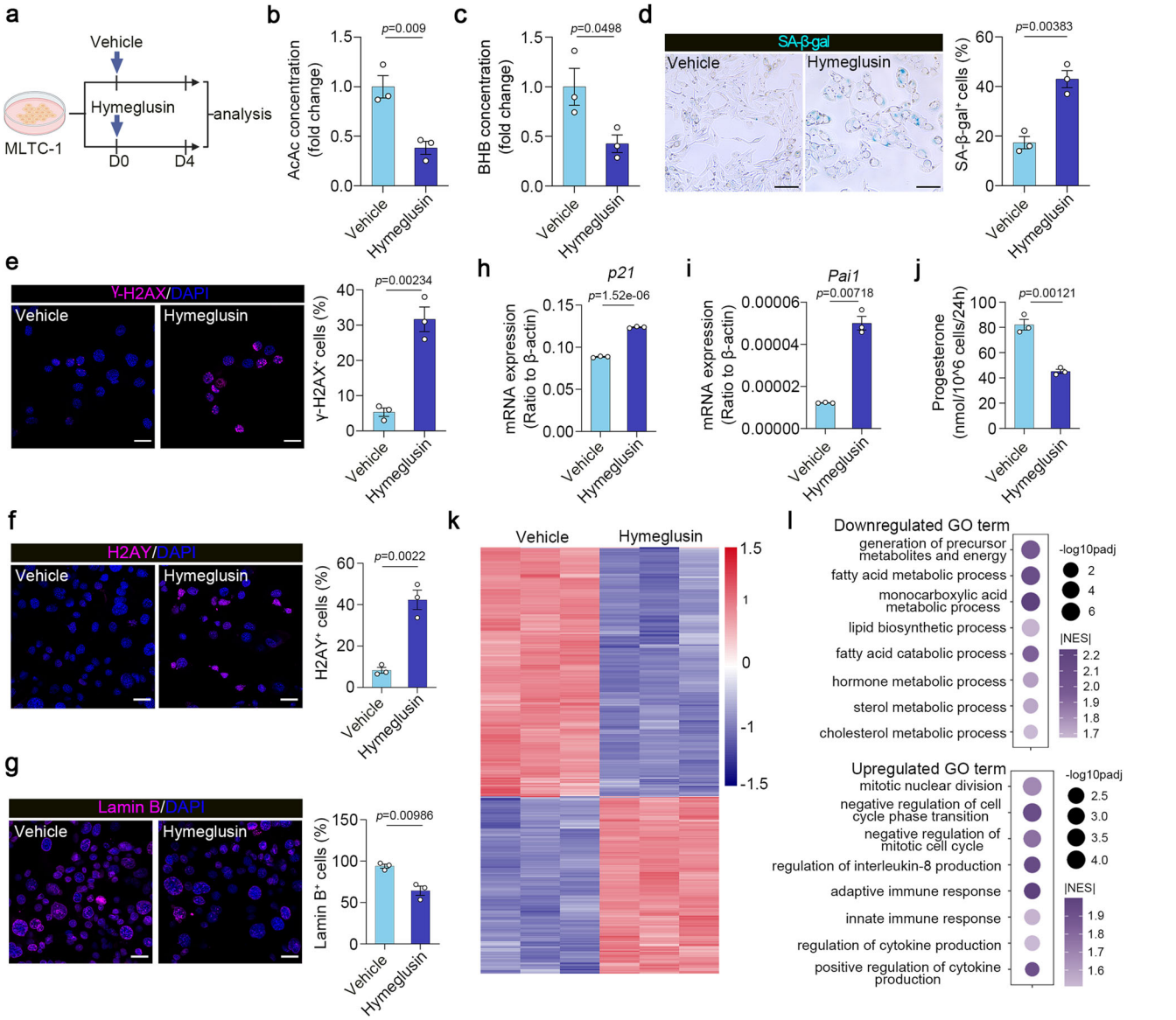

Fig. 3 | Inhibition of Hmgcs2 accelerates senescence of Leydig cells. a Schematic of the experimental workflow. **b, c** The level of ketone bodies in MLTC-1 cells. $n = 3$ per group. Cells were treated with Hymeglusin (3 μM) for 4 days before analysis of ketone bodies. **d** Left: representative images of SA-β-gal (senescence-associated β-galactosidase) staining. Scale bar: 75 μm. Right: quantitative analysis of the SA-β-gal$^+$ cells. Cells were treated with Hymeglusin (3 μM) for 4 days before SA-β-gal staining. $n = 3$ per group. **e** Left: representative images of γ-H2AX (phosphorylated H2AX) staining. Scale bar: 25 μm. Right: quantitative analysis of the γ-H2AX$^+$ cells. Cells were treated with Hymeglusin (3 μM) for 4 days before staining. $n = 3$ per group. **f** Left: representative images of H2AY (histone protein macroH2A.1) staining. Scale bar: 25 μm. Right: quantitative analysis of the H2AY$^+$ cells. Cells were treated with Hymeglusin (3 μM) for 4 days before staining. $n = 3$ per group. **g** Left: representative images of Lamin B staining. Scale bar: 25 μm. Right: quantitative analysis of the Lamin B$^+$ cells. Cells were treated with Hymeglusin (3 μM) for 4 days before staining. $n = 3$ per group. **h, i** Quantitative RT-PCR analysis of senescence markers (*p21*, *Pai1*). Cells were treated with Hymeglusin (3 μM) for 4 days before analysis. $n = 3$ per group. **j** Progesterone production of MLTC-1 cells. Cells were exposed to Hymeglusin (3 μM) for 4 days before analysis. $n = 3$ per group. **k** Heat map of differentially expressed genes in Hymeglusin-treated and control groups. **l** Upregulated or downregulated GO terms of Hymeglusin-treated MLTC-1 cells, with the dot size indicating the range of −log10 (adjusted *P*-value). Color keys, ranging from grey to blue, indicate the absolute value of the NES. Data were presented as mean ± SEM. Significance was determined by Two-tailed t-test (**b**–**j**) or Two-sided permutation test with BH correction (**l**). n represents the number of biological replicates in (**b**–**j**). Illustrations were created with BioRender. Source data are provided as a Source Data file.

(Fig. 4k), while serum LH concentrations increased in AAV-Cre treated mice (Fig. 4l). Furthermore, histological analysis showed thinning of the seminiferous epithelium in AAV-Cre treated mice (Fig. 4m–o). Sperm analysis indicated a decrease in sperm concentration in AAV-Cre treated mice compared to AAV-GFP treated mice, however, no significant difference was detected in sperm motility or progressive motility between the two groups (Fig. 4p–s). These findings indicate that ketogenesis exerts protective effects on LCs, and loss of *Hmgcs2* leads to premature senescence of LCs and accelerates testicular aging.

The protective effects of ketogenesis on LCs are mediated by BHB but not AcAc

To determine which ketogenic products contribute to the protective effects of ketogenesis on LCs, we examined their ability to mitigate cellular senescence caused by HMGCS2 inhibition or silence. Our results demonstrated that BHB (5 mM) alleviated Hymeglusin-induced cellular senescence, as evidenced by the reduced proportion of SA-β-gal$^+$ cells (Supplementary Fig. 5a) and the downregulation of senescence markers p16 and p53 (Supplementary Fig. 5b). Moreover, quantitative RT-PCR analysis showed

https://doi.org/10.1038/s41467-025-59591-8

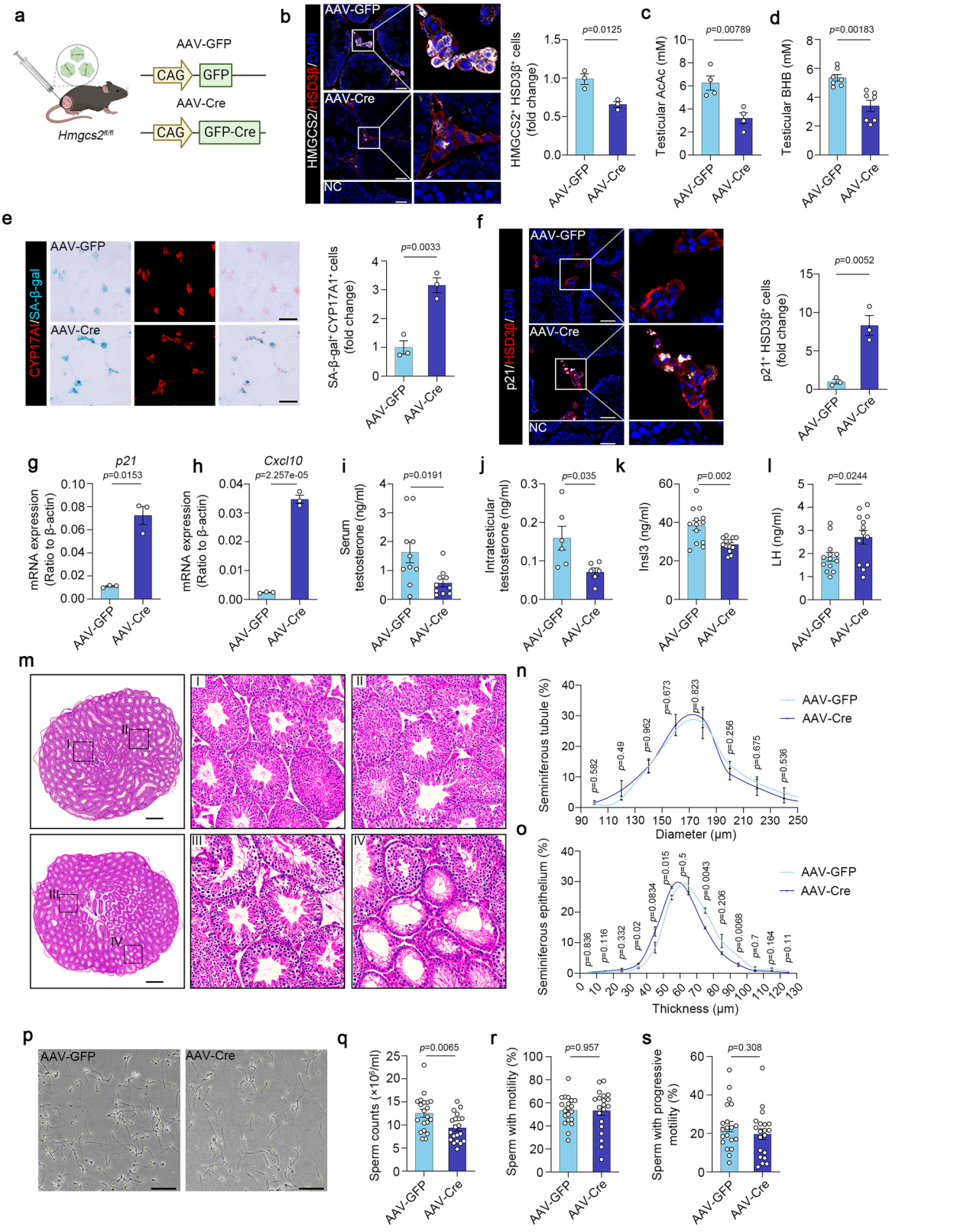

that BHB decreased the expression of *p21* and *Pai1* (Supplementary Fig. 5c, d). However, AcAc (5 mM) had no effect on the senescence of Hymeglusin-treated MLTC-1 cells and, in some cases, even appeared to exacerbate senescence (Supplementary Fig. 5a–d). Consistent with these findings, BHB restored the steroidogenic function impaired by Hymeglusin, as demonstrated by increased progesterone levels in the culture medium supernatant, whereas AcAc offered no such protective effect (Supplementary Fig. 5e). Similarly, BHB attenuated *Hmgcs2*-knockdown-induced cellular senescence, as indicated by the reduced proportion of SA-β-gal⁺ cells (Supplementary Fig. 5f, g) and decreased *p21* and *Pai1* expression (Supplementary Fig. 5h–k). Collectively, these findings suggest that BHB mediates the protective effects of ketogenesis on LCs.

Fig. 4 | Conditional knockout of *Hmgcs2* in LCs leads to testicular aging in young mice. a Schematic of AAV (adeno-associated virus) mediated *Hmgcs2* conditional knockout. **b** Left: 4 weeks post-injection, representative testicular sections from AAV-GFP and AAV-Cre infected mice, stained with LCs marker HSD3β, HMGCS2, and DAPI. NC: negative control. Scale bar: 50μm. Right: quantitative analysis of HMGCS2$^+$ HSD3β$^+$ cells. $n = 3$ per group. **c, d** 4 weeks post-injection, testicular AcAc and BHB concentration in AAV-GFP and AAV-Cre infected mice. $n = 4$ per group in (**c**), $n = 7$ per group in (**d**). **e** Left: 2 months post-injection, representative testicular sections from AAV-GFP and AAV-Cre infected mice, stained with LCs marker CYP17A1, and SA-β-gal. Scale bar: 75 μm. Right: quantitative analysis of CYP17A1$^+$ SA-β-gal$^+$ cells. $n = 3$ per group. **f** Left: 2 months post-injection, representative testicular sections from AAV-GFP and AAV-Cre infected mice, stained with senescence marker p21, HSD3β, and DAPI. NC: negative control. Scale bar: 50 μm. Right: quantitative analysis of p21$^+$ HSD3β$^+$ cells. $n = 3$ per group. **g, h** 2 months post-injection, quantitative RT-PCR analysis of senescence markers (*p21*, *Cxcl10*) in AAV infected LCs. $n = 3$ per group. **i–l** Serum testosterone (**i**), intratesticular testosterone (**j**), serum Insl3 (Insulin-like peptide 3) (**k**), serum LH (Luteinizing Hormone) (**l**) level of the indicated groups. $n = 10$ per group in (**i**), $n = 6$ per group in (**j**), $n = 13$ per group in (**k**), $n = 13$ per group in (**l**). **m–o** 2 months post-injection, representative HE (hematoxylin-eosin) stained testicular sections obtained from AAV-GFP and AAV-Cre infected mice. Scale bar: 500 μm (**m**). The percentages of seminiferous tubules with varying diameters (**n**) and epithelial thickness (**o**). $n = 3$ per group. **p** Representative light micrographs of sperm acquired from indicated groups. Scale bar: 100 μm. **q–s** Sperm concentration (**q**), proportion of sperm with motility (**r**), proportion of sperm with progressive motility (**s**). $n = 20$ per group. Data were presented as mean ± SEM. Significance was determined by Two-tailed t-test. Illustrations were created with BioRender. Source data are provided as a Source Data file.

Next, we investigated whether ketogenic metabolites confer protection against senescence induced by common stressors[31]. Hydrogen peroxide (H_2O_2) triggers premature senescence by increasing oxidative stress[32]. As expected, H_2O_2 (100 μM) exposure increased the number of SA-β-gal$^+$ cells and led to a significant decline in *Hmgcs2* transcripts in MLTC-1 cells (Fig. 5a, b; Supplementary Fig. 6a). Treatment with BHB (5 mM) decreased SA-β-gal$^+$ cells and lowered expression of senescence markers *p21* and *Cxcl10* (Fig. 5b–e). Additionally, BHB restored progesterone levels impaired by H_2O_2, whereas AcAc (5 mM) had no protective effect (Fig. 5f). Similarly, doxorubicin (DXR, 150 nM), a chemotherapeutic agent known to induce senescence[33], increased SA-β-gal$^+$ cells and significantly reduced *Hmgcs2* expression (Supplementary Fig. 6b,e). BHB alleviated DXR-induced senescence by decreasing SA-β-gal$^+$ cells and suppressing the expression of *p21* and *Pai1*, while AcAc showed no effect (Supplementary Fig. 6d–g). Lastly, ionizing radiation (IR, 8 Gy), which induces senescence through DNA damage[34], also resulted in downregulation of *Hmgcs2* expression and an increase in SA-β-gal$^+$ cells in MLTC-1 cells (Supplementary Fig. 6c). Treatment with BHB significantly reduced SA-β-gal$^+$ cells and downregulated senescence markers *p21* and *Cxcl10*, whereas AcAc remained ineffective (Supplementary Fig. 6h–k). Collectively, these results demonstrate that BHB consistently mitigates senescence induced by oxidative stress, chemotherapy, and radiation, underscoring its protective role in LCs.

BHB alleviates testicular aging by enhancing histone acetylation

We next elucidate the molecular mechanism by which BHB alleviates LCs senescence. Recent studies have suggested that BHB acts as an epigenetic modifier, particularly by altering histone H3 at lysine 9 (H3K9) through β-hydroxybutyrylation (Kbhb)[35]. However, our findings demonstrate that BHB treatment did not increase the Kbhb of H3K9 in MLTC-1 cells, thereby excluding the possibility that BHB regulates senescence via Kbhb (Fig. 5g). In addition to Kbhb, BHB serves as an endogenous inhibitor of histone deacetylase (HDAC), thereby modulating H3K9 acetylation (H3K9ac)[36]. Western blot and immunofluorescence staining analyses revealed that H3K9ac was dose-dependently upregulated by BHB in MLTC-1 cells (Fig. 5g, h), consistent with its role as a potential HDAC inhibitor. To verify that BHB alleviates LCs senescence by inhibiting HDAC, we first demonstrated that BHB treatment reduced HDAC activity in MLTC-1 cells, similar to the pharmacological inhibitor vorinostat (Fig. 5i). Then, senescent MLTC-1 cells were treated with BHB (5 mM) or vorinostat (1 μM). Both treatments reduced the number of SA-β-gal$^+$ cells (Fig. 5j) and decreased the expression of senescence markers *p16*, *p21*, and *Cxcl10* (Fig. 5k–m). Additionally, BHB and vorinostat individually increased progesterone concentration in the supernatant of the culture medium (Fig. 5n). However, co-treatment with vorinostat and BHB did not further increase progesterone concentrations or decrease the expression of senescence markers, indicating redundancy between BHB signaling and HDAC inhibition (Fig. 5j–n). These data support that BHB mitigates cell senescence by enhancing histone acetylation via HDAC inhibition.

BHB-mediated HDAC1 inhibition enhances *Foxo3a* expression

BHB is as an endogenous inhibitor of HDAC1, HDAC2, and HDAC3[27,37]. To identify which HDAC subtype mediates the alleviation of cell senescence by BHB, we conducted a focused analysis of the LCs cluster from scRNA-seq data. This analysis revealed that the expression of *Hdac1* in LCs from aged mice is higher than that in young mice (Supplementary Fig. 7a). Then, we performed quantitative RT-PCR and found that *Hdac1* expression increased significantly in the aged group, while *Hdac2* and *Hdac3* expressions were comparatively lower, with no significant differences between the groups (Supplementary Fig. 7b).

To determine whether the protective effect of BHB required *Hdac1* expression, we applied shRNA to knockdown *Hdac1* in MLTC-1 cells (Supplementary Fig. 7c). As expected, silencing of *Hdac*1 in MLTC-1 cells abrogated the ability BHB to alleviate senescence. Specifically, BHB treatment did not reduce the proportion of SA-β-gal$^+$ cells in the *Hdac*1-silenced group (Supplementary Fig. 7d, e). Similarly, quantitative RT-PCR analysis showed that BHB treatment failed to decrease the expression of senescence markers *p21* and *Cxcl10* in *Hdac1*-silenced cells (Supplementary Fig. 7f, g). Furthermore, gene silencing of *Hdac1* prevented BHB from enhancing steroidogenic function of MLTC-1 cells (Supplementary Fig. 7h). These results suggest that BHB mitigates senescence primarily by inhibiting HDAC1.

Histone acetylation induced by BHB is associated with the transcriptional activation of genes[36]. FOXO3a, a longevity-associated transcription factor, has been reported to be upregulated by BHB-mediated histone acetylation[36,38]. To investigate the role of *Foxo3a* in LCs senescence, we performed Western blot analysis, which demonstrated that FOXO3a expression is downregulated in H_2O_2-induced senescent MLTC-1 cells. As expected, BHB treatment upregulated the expression of FOXO3a (Supplementary Fig. 8a). To assess whether BHB alleviates cell senescence through *Foxo3a* pathway, we applied shRNA to knockdown *Foxo3a* in MLTC-1 cells (Supplementary Fig. 8b). SA-β-gal staining showed that *Foxo3a* silencing invalidated the BHB's ability to alleviate senescence (Supplementary Fig. 8c, d). Similarly, quantitative RT-PCR analysis showed that BHB treatment did not decrease the expression of senescence markers *p21* and *Cxcl10* in *Foxo3a*-silenced cells (Supplementary Fig. 8e, f). To demonstrate that *Foxo3a* expression is regulated by HDAC1, we conducted chromatin immunoprecipitation-qPCR (ChIP-qPCR) analysis, which showed that BHB restored histone H3K9 acetylation at the *Foxo3a* promoter in MLTC-1 cells (Supplementary Fig. 8g). Furthermore, *Hdac1* knockdown significantly increased *Foxo3a* expression, indicating that BHB upregulates *Foxo3a* expression by inhibiting HDAC1 (Supplementary Fig. 8h). These results demonstrate that BHB promotes *Foxo3a* expression by inhibiting HDAC1 activity, thereby mitigating cell senescence.

https://doi.org/10.1038/s41467-025-59591-8

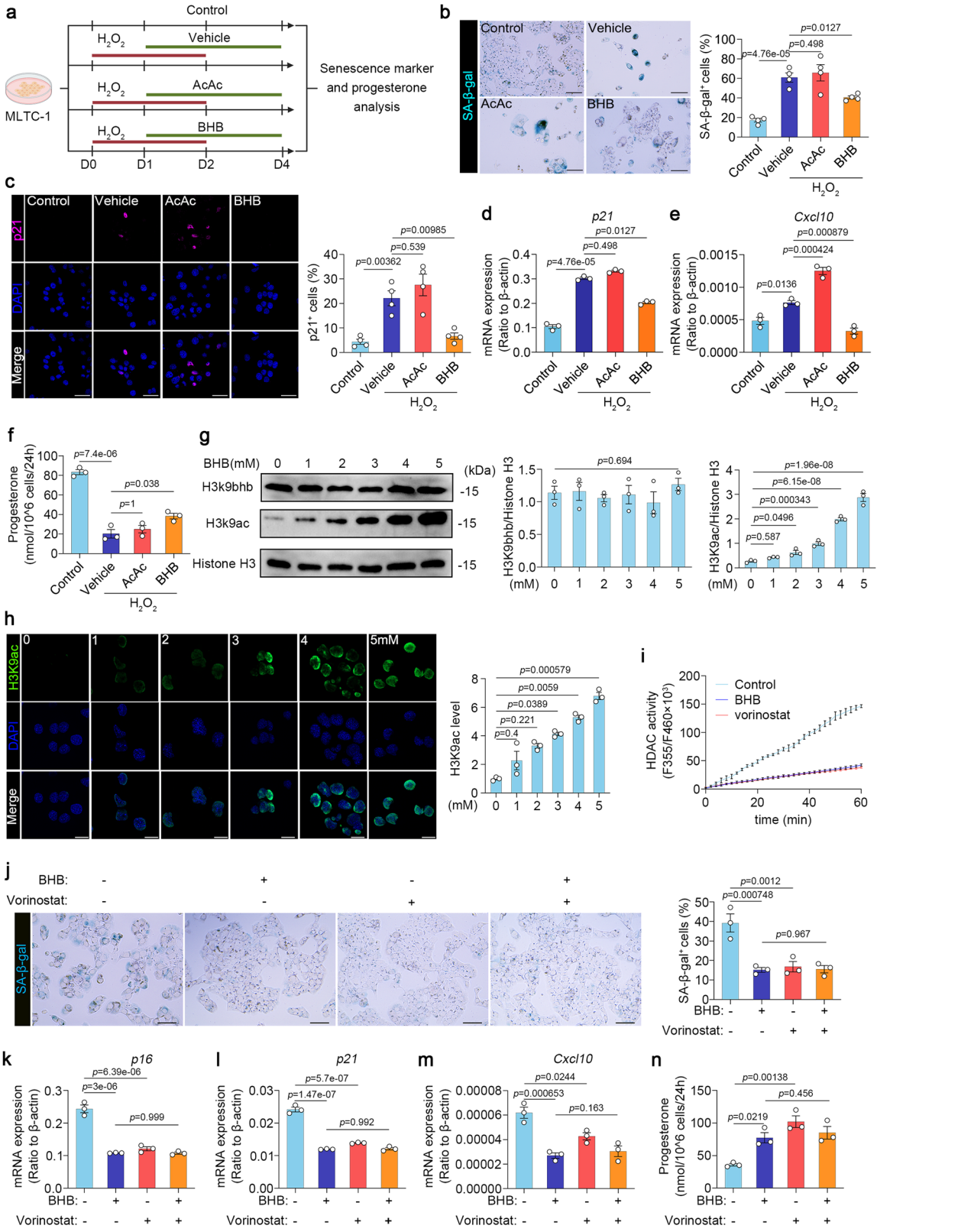

Previous reports have shown that FOXO3a can exert anti-aging effects by inhibiting inflammation or promote DNA repair[36,39,40]. To further investigate these possibilities, we sorted LCs from young (2-month-old) and aged (24-month-old) mice and performed bulk RNA sequencing. The analysis revealed that *Foxo3a* expression was significantly downregulated in LCs from aged mice, accompanied by a downregulation of DNA repair genes (Supplementary Fig. 9a). In contrast, inflammation-related genes were significantly upregulated in LCs from aged mice (Supplementary Fig. 9a).

Enhancement of ketogenesis alleviates LCs senescence and testicular aging in aged mice

Given that BHB exhibits protective effects on LCs in vitro, we asked whether overexpression of *Hmgcs2* in LCs of aged mice could exert an

Fig. 5 | BHB alleviates cellular senescence by promoting histone acetylation via HDAC inhibition. a Experimental scheme of H_2O_2 (hydrogen peroxide) induced senescence, AcAc (5 mM) or BHB (5 mM) treatment and analysis. **b** Left: representative images of SA-β-gal staining in MLTC-1 cells of the indicated groups. Scale bar: 75 μm. Right: quantitative analysis of the SA-β-gal$^+$ cells. $n = 4$ per group. **c** Left: representative images of senescence marker p21 in MLTC-1 cells of the indicated groups. Scale bar: 25μm. Right: quantitative analysis of the p21$^+$ cells. $n = 4$ per group. **d, e** Quantitative RT-PCR analysis of senescence marker (*p21*, *Cxcl10*) in the indicated groups. $n = 3$ per group. **f** Progesterone production of MLTC-1 cells. $n = 3$ per group. **g** Right: Representative western blots for H3K9bhb and H3K9ac and Histone H3. Left: quantitative analysis of H3K9bhb and H3K9ac protein levels. Relative to Histone H3. MLTC-1 cells were treated with BHB (0, 1, 2, 3, 4, 5 mM) for 24 h before analysis. $n = 3$ per group. **h** Left: representative images of H3H9ac staining in MLTC-1 cells treated with BHB for 24 h. Scale bar: 20μm. Right: quantitative analysis of fluorescence intensity. $n = 3$ per group. **i** HDAC activity in MLTC-1 cells treated with BHB (5 mM) or vorinostat (1 μM). $n = 3$ per group. **j** Left: representative images of SA-β-gal staining in MLTC-1 cells of the indicated groups. Senescent cells were treated with BHB (5 mM) or vorinostat (1 μM) for 48 h before staining. Scale bar: 75μm. Right: quantitative analysis of the SA-β-gal$^+$ cells. $n = 3$ per group. **k**–**m** Quantitative RT-PCR analysis of senescence markers (*p16*, *p21*, *Cxcl10*) in the indicated groups. Senescence cells were treated with BHB (5 mM) or vorinostat (1 μM) for 48 h before analysis. $n = 3$ per group. **n** Progesterone production of MLTC-1 cells. Senescent cells were treated with BHB (5 mM) or vorinostat (1 μM) for 48 h before analysis. $n = 3$ per group. Data were presented as mean ± SEM. Significance was determined by one-way ANOVA (**b**–**g**, **j**–**n**) or Kruskal-Wallis test (**h**). *n* represents the number of biological replicates in (**b**–**g**, **j**–**n**). Illustrations were created with BioRender. Source data are provided as a Source Data file.

anti-aging effect on testicular function. To test this hypothesis, we used AAV vectors to deliver and overexpress the *Hmgcs2* gene (AAV-Hmgcs2, O.E.) or mCherry (AAV-mCherry, Con) under the control of the CAG promoter in the testes of aged mice (15-month-old) (Fig. 6a). Immunofluorescence staining confirmed a significant increase in HMGCS2 expression 2 weeks after testicular injection of AAV-*Hmgcs2* (Fig. 6b). Additionally, analysis of ketogenic products revealed a marked increase of BHB in AAV-*Hmgcs2* treated testes, approaching the BHB levels observed in young testes (Fig. 6c). Consistent with in vitro results, Western blot analysis demonstrated that *Hmgcs2* overexpression increased the levels of H3K9ac and FOXO3a in aged testicular tissue, similar to the levels in young testes (Fig. 6d, e).

Next, we determined whether *Hmgcs2* overexpression alleviates LCs senescence. Overexpression of *Hmgcs2* resulted in a significant decrease in the number of SA-β-gal$^+$ LCs in aged mice (Fig. 6f). Immunofluorescence analysis revealed a significant decrease of the senescence marker p21 in LCs from AAV-*Hmgcs2*-treated mice (Fig. 6g). Quantitative RT-PCR analysis showed that *Hmgcs2* overexpression significantly downregulated senescence markers *p21* and *Cxcl10* (Fig. 6h, i). Additionally, serum and intratesticular testosterone concentrations increased significantly in AAV-*Hmgcs2*-treated mice compared to AAV-mCherry-treated mice (Fig. 6j, k). The increase in Insl3 concentrations and decrease in serum LH concentrations further suggested the improved LCs function in AAV-*Hmgcs2*-treated mice (Fig. 6l, m). These results indicate that overexpression of *Hmgcs2* alleviates senescence and improves the function of LCs in vivo.

We then investigated whether overexpression of *Hmgcs2* in LCs could improve spermatogenesis. Four weeks after AAV-*Hmgcs2* injection, histological analysis revealed enlarged diameters of seminiferous tubules and increased thickness of seminiferous epithelium (Fig. 6n–p). Sperm analysis demonstrated that *Hmgcs2* overexpression significantly increased sperm concentration in aged mice. However, no significant differences were observed in sperm motility and progressive motility between two groups (Fig. 6q–t). Last, we validated the changes in FOXO3a-related inflammation genes through quantitative RT-PCR analysis, revealing that inflammation-related genes were significantly upregulated in aged mice, and *Hmgcs2* overexpression reduced the expression of these genes (Supplementary Fig. 9b–e). Overall, these data suggest that enhancing ketogenesis is sufficient to alleviate LCs senescence and testicular aging in aged mice.

Oral BHB treatment improves testicular function in aged mice

We next investigated whether dietary BHB has a beneficial effect on testicular aging in aged mice (18-month-old). A 10 ml BHB salt formulation (KetoForce) was administered in 290 ml of drinking water and mix thoroughly. The KetoForce solution consists of BHB salt with 1.6 g sodium and potassium per 11.7 g BHB. Control cohorts received water supplemented with molar equivalents of the salts presented in the BHB supplement (Fig. 7a). All treated animals consumed comparable amounts of food and water (Fig. 7b). The result showed that oral BHB increased BHB levels in both the serum and testes of aged mice (Fig. 7c). Consistent with in vitro results, Western blot analysis revealed that BHB increased the levels of H3K9ac and FOXO3a in aged testicular tissue, similar to the levels observed in young testes (Fig. 7d, e).

After eight weeks of treatment, oral BHB resulted in a significant decrease in the number of SA-β-gal$^+$ LCs in the testes of aged mice (Fig. 7f). Immunofluorescence analysis revealed a decrease in the senescence marker p21 in LCs from the BHB-treated mice (Fig. 7g). Quantitative RT-PCR analysis showed that oral BHB significantly downregulated *p21* and *Cxcl10* (Fig. 7h, i). Additionally, serum and intratesticular testosterone levels were significantly increased in the BHB-treated group (Fig. 7j, k). Furthermore, the increase in Insl3 concentrations and the decrease in serum LH concentrations confirmed the improvement of endocrine function of testes in BHB-treated mice (Fig. 7l, m). However, sperm analysis showed no significant differences in sperm concentration, sperm motility, or progressive motility between control and experimental cohorts (Fig. 7n–q). Subsequently, we validated the changes in FOXO3a-related inflammation genes through quantitative RT-PCR analysis, revealing that inflammation-related genes were significantly upregulated in aged mice and BHB supplementation reduced the expression of these genes (Supplementary Fig. 9f–i). Collectively, these results suggest that dietary BHB can alleviate the senescence of LCs and mitigate testicular aging.

Discussion

While previous studies have addressed the mechanisms of testicular aging[41,42], a comprehensive understanding of its driving forces remains elusive. Given that senescent cells drive organ dysfunction and aging process, we first aimed to characterize the senescent profile of testicular cells during aging in mice. Utilizing SA-β-gal staining, we observed that senescent cells predominantly localize to the testicular interstitium. Among interstitial cells, LCs produce testosterone and are thus critical for reproductive function and general health[43]. LCs dysfunction leads to testosterone deficiency, arrested spermatogenesis, and infertility[44,45]. By co-staining SA-β-gal with specific cell markers, we identified LCs as the earliest cell type to exhibit signs of cell senescence in the testis, which is evident as early as 8 months of age in mice. Our histological analysis further revealed a notable increase in p21, a well-established marker of senescence, in LCs from aged mice[46]. Accordingly, LCs produce a large amount of ROS when synthesized testosterone, making them vulnerable to ROS-induced damage[47]. Moreover, LCs are long-living cells that exist throughout the male's life, which exposes LCs to age-accumulated damage[43]. Based on these findings, we speculated that the intrinsic properties of LCs render them particularly susceptible to aging insults.

To further investigate the characteristics of LCs in aging, we conducted scRNA-seq analysis, revealing notable transcriptomic changes in aged LCs. Intriguingly, *Hmgcs2*, the gene encoding the rate-limiting enzyme in ketone bodies production[27], was significantly

https://doi.org/10.1038/s41467-025-59591-8

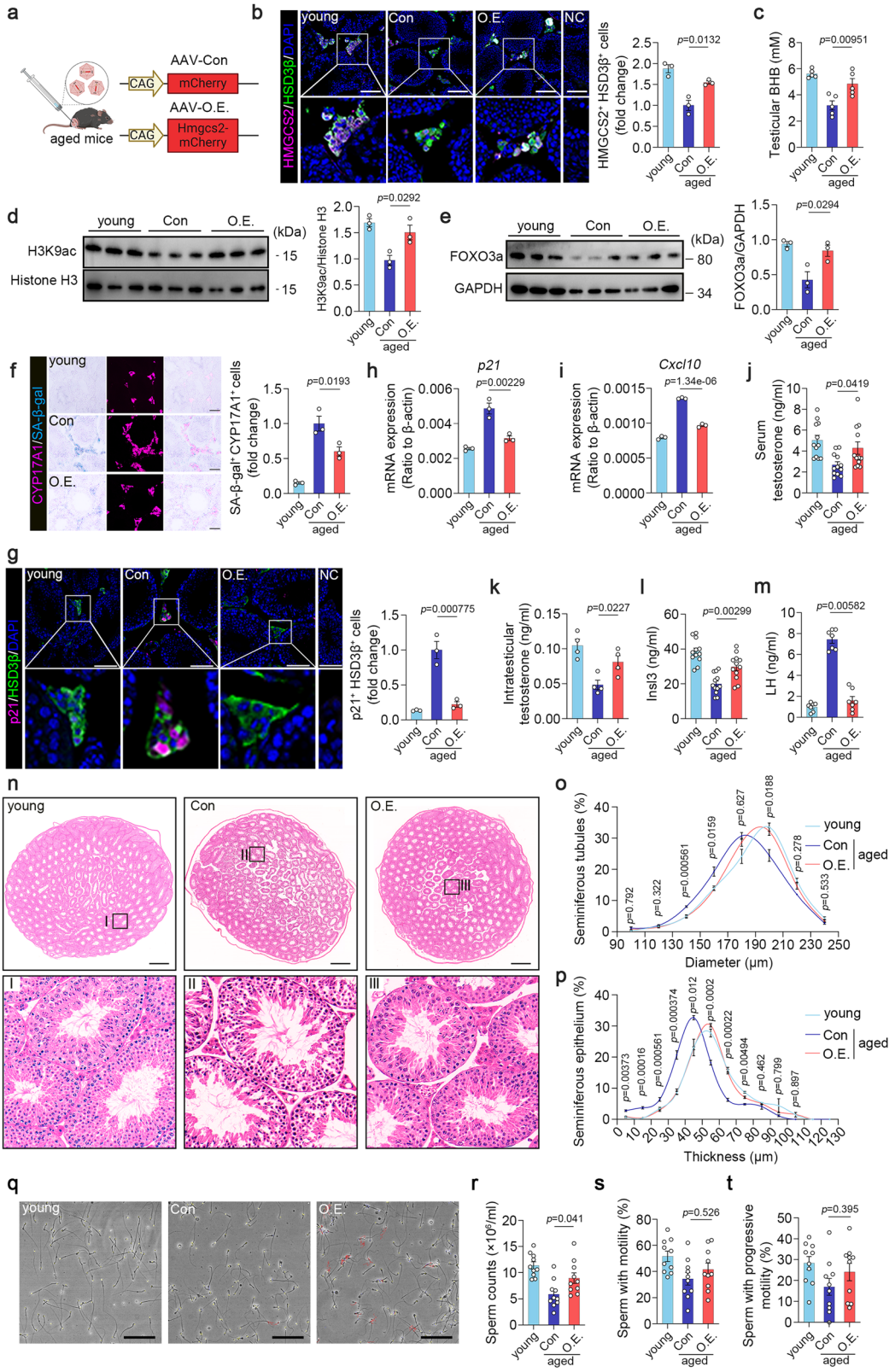

downregulated in aged LCs. Consistently, intratesticular ketone bodies (BHB and AcAc) concentrations were markedly decreased in aged testes compared to those in young testes. Ketone bodies are produced in the liver during conditions of reduced carbohydrate availability and serve as an alternative fuel source for peripheral tissues including brain, heart and skeletal muscle[28,48,49]. However, their role in the testes has not been systematically studied. Surprisingly, the concentration of ketone bodies in the testes were more than tenfold higher than that in serum, indicating that intratesticular ketogenesis is likely a key event for maintaining testicular homeostasis. Recent studies have reported that local ketogenesis is essential for tissue repair[27,50]. For example, proximal tubular epithelial cells in the kidney could produce ketone bodies to attenuate podocyte damage and proteinuria in diabetic mice[51]. Similarly, in the mammalian small intestine, the expression of

Fig. 6 | Enhancing ketogenesis in LCs of aged mice alleviates testicular aging. **a** Schematic of AAV-mediated *Hmgcs2* overexpression. **b** Left: 2 weeks post-injection, representative testicular sections from AAV-Control and AAV-O.E. infected mice, stained with LCs marker HSD3β, HMGCS2, and DAPI. NC: negative control. Scale bar: 50μm. Right: quantitative analysis of HMGCS2$^+$ HSD3β$^+$ cells. $n = 3$ per group. **c** Testicular BHB concentration 2 weeks post-injection. $n = 5$ per group. **d** Left: 2 weeks post-injection, representative western blots for H3K9ac and Histone H3 in testes of different mice. Right: quantitative analysis of H3K9ac protein level, relative to Histone H3. $n = 3$ per group. **e** Left: 2 weeks post-injection, representative western blots for FOXO3a and GAPDH in testes of different mice. Right: quantitative analysis of FOXO3a protein level, relative to GAPDH. $n = 3$ per group. **f** Left: 2 months post-injection, representative testicular sections from different mice stained with LC marker CYP17A1, and SA-β-gal. Scale bar: 75μm. Right: quantitative analysis of CYP17A1$^+$ SA-β-gal$^+$ cells. $n = 3$ per group. **g** Left: 2 months post-injection, representative testicular sections from different mice stained with senescence marker p21, HSD3β, and DAPI. Scale bar: 50μm. Right: quantitative analysis of p21$^+$ HSD3β$^+$ cells. $n = 3$ per group. **h, i** 2 months post-injection, quantitative RT-PCR analysis of senescence markers (*p21, Cxcl10*) in LCs. $n = 3$ per group. **j**–**m** Serum testosterone (**j**), intratesticular testosterone (**k**), serum Insl3 (**l**), serum LH (**m**) level of the indicated groups. $n = 12$ per group in (**j**), $n = 4$ per group in (**k**), $n = 12$ per group in (**l**), $n = 7$ per group in (**m**). **n**–**p** 2 months post-injection, representative HE stained testicular sections. Scale bar: 500 μm (**n**). The percentages of seminiferous tubules with varying diameters (**o**) and epithelial thickness (**p**). $n = 3$ per group. **q**–**t** Representative light micrographs of sperm from the indicated groups. Scale bar: 100 μm (**q**). Sperm concentration (**r**), proportion of sperm with motility (**s**), proportion of sperm with progressive motility (**t**). $n = 10$ per group. Data were presented as mean ± SEM. Significance was determined by one-way ANOVA (**b**–**i, k, l, o**–**t**) or Kruskal-Wallis test (**j**, **m**). Illustrations were created with BioRender. Source data are provided as a Source Data file.

Hmgcs2 distinguishes self-renewing Lgr5$^+$ stem cells (ISCs) from differentiated cell types. Loss of *Hmgcs2* depletes ketone bodies levels in Lgr5$^+$ ISCs and skews their differentiation toward secretory cell fates[27]. Our present study revealed that silencing *Hmgcs2* expression in LCs impaired ketogenesis, consequently inducing premature senescence of LCs and accelerating testicular aging. Interestingly, this knockout specifically affected ketone body levels within the testis without altering serum levels. These results strongly suggest that the early onset of LCs senescence is likely attributed to declined ketogenesis.

Ketone bodies include AcAc and its redox partner BHB[28]. While AcAc showed protective effects against liver fibrosis and Duchenne muscular dystrophy[52,53], it did not confer benefits to senescent LCs in our study. In contrast, BHB exhibited a geroprotective effect on senescent LCs. BHB serves not only a ketogenic metabolite for energy supply but also acts as an epigenetic modifier, including H3K9 acetylation or Kbhb[35,36]. However, BHB treatment did not increase H3K9 Kbhb in MLTC-1 cells, thereby excluding the possibility that BHB functions as an β-hydroxybutyryl donor for lysine β-hydroxybutyrylation of H3K9. Notably, BHB treatment dose-dependently enhanced H3K9ac modifications, suggesting that BHB acts as endogenous histone deacetylase inhibitor to modulate H3K9 acetylation. In addition, BHB inhibited HDAC activity in MLTC-1 cells, comparable to the pharmacological HDAC inhibitor vorinostat. Consistent with this, co-treatment with HDAC inhibitor vorinostat and BHB did not further alleviate senescence or increase progesterone concentrations, indicating redundancy between BHB signaling and HDAC inhibition. Our study further confirmed that HDAC1 plays a significant role in LCs senescence, as inactivation of HDAC1 by shRNA undermined the therapeutic effect of BHB on LCs senescence. *Foxo3a* is ubiquitously expressed across the body and associated with healthspan and longevity[54,55]. It has been reported that downregulation of *Foxo3a* is associated with physiological vascular aging in aged primates[56]. Similarly, we found that *Foxo3a* is downregulated in senescent MLTC-1 cells, which can be reversed by BHB treatment. Meanwhile, we found that treatment of MLTC-1 cells with BHB led to increased H3K9ac acetylation at the *Foxo3a* promoters. However, upon *Hdac1* knockdown, BHB failed to enhance *Foxo3a* levels, indicating that BHB upregulates *Foxo3a* expression by inhibiting HDAC1. Moreover, loss of *Foxo3a* could directly trigger MLTC-1 cells senescence, which could not be alleviated by BHB treatment, supporting the notion that BHB alleviates LCs senescence by promoting *Foxo3a* expression.

Notably, the present study revealed that overexpression of *Hmgcs2* in the LCs of aged mice significantly increased BHB levels and mitigated testicular dysfunction, indicating targeted interventions for LCs senescence showed promise in delaying testicular aging. Previous studies have reported different interventions to induce ketogenesis, including fasting, ketogenic diet, and direct oral BHB administration[57,58]. Dietary interventions to induce ketosis, such as fasting and ketogenic diet, are not costly and appear relatively safe[59,60]. Unfortunately, dietary interventions most frequently fail as therapies due to inability of individuals to adhere to the diets[61]. Our findings provide evidence that oral BHB treatment effectively increases testosterone levels and partially mitigates testicular aging, without the need for the significant lifestyle changes required by fasting or ketogenic diets. This approach offers a more feasible therapeutic option for testicular aging. Our results support the notion that either enhancing endogenous ketone body production in LCs or supplementing with exogenous ketone bodies can effectively alleviate aging in mouse testes. Considering the potential health risks associated with exogenous testosterone replacement therapy[7–10], the use of ketone body supplementation offers a viable and promising alternative for counteracting testicular aging.

In the present study, we did not perform fertility assessments due to limited availability of aged mice. However, our study found that enhancing BHB levels achieved significant improvements in the testosterone levels in aged mice. Notably, the sperm concentrations were significantly restored in AAV-*Hmgcs2* treated mice. Due to these remarkable enhancements in testosterone production and sperm parameters, we speculate the treated aged mice may exhibit improved fertility, which needs further evaluation in future studies. Furthermore, the role of *Foxo3a* in the testis warrants further investigation. *Foxo3a* is widely recognized as a broad-spectrum transcription factor involved in regulating various physiological and pathological processes, including inhibit inflammation, oxidative stress, and promote DNA damage repair, all of which may contribute to testicular aging[62–64]. However, *Foxo3a* regulates distinct downstream target genes in a cell type-dependent manner[65], its role in testicular aging remains to be clarified in future studies.

In conclusion, our study demonstrated that LCs are the most susceptible cells to aging in the testis and identified *Hmgcs2* as a vital downregulated gene in LCs with aging. Moreover, knockout of *Hmgcs2* in young LCs impaired ketogenesis in testis, driving senescence of LCs and inducing testicular aging. Conversely, the activation of ketogenesis, as enhanced by genetic manipulation or dietary intervention, alleviates LCs senescence and restores testicular functions, positioning ketogenesis enhancement as a promising therapeutic strategy for delaying testicular aging. Our findings deepen the understanding of testicular aging by highlighting the pivotal role of ketogenesis in maintaining testicular homeostasis, thereby suggesting specific avenues for understanding and potentially mitigating testicular aging.

Methods

Animals

All mice were bred on a C57BL/6 background and raised in a specific pathogen-free (SPF) environment. Wild-type mice were purchased

https://doi.org/10.1038/s41467-025-59591-8

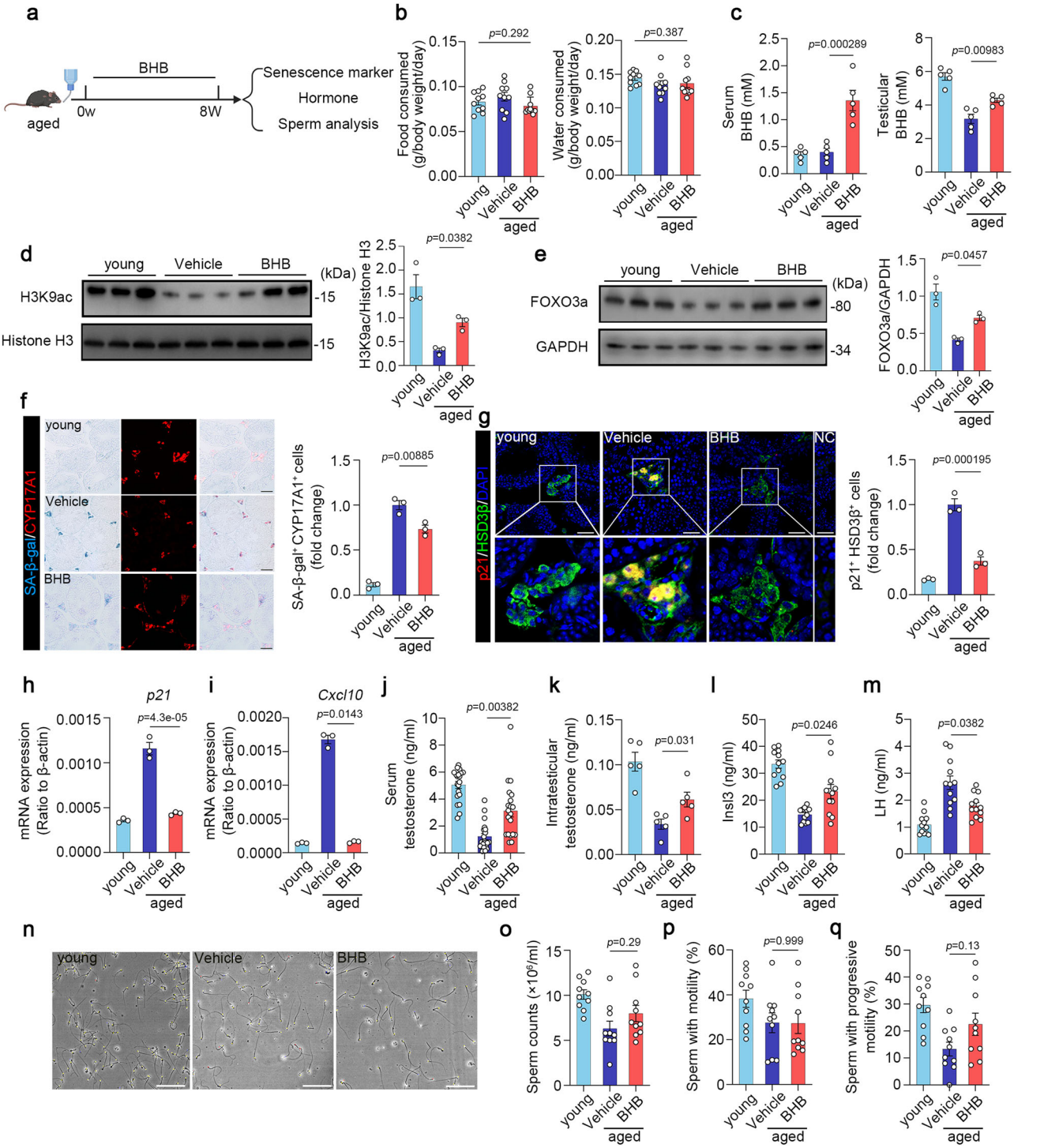

Fig. 7 | Oral administration of BHB partially alleviates testicular aging in aged mice. a Schematic of oral administration of BHB and subsequent analysis. **b** Water and food consumption between salt and BHB-treated mice. $n = 10$ per group. **c** The concentration of BHB in serum and testes. $n = 5$ per group. **d** Left: the representative western blots for H3K9ac and Histone H3 in testes of different mice. Right: quantitative analysis of the H3K9ac protein level, relative to Histone H3. $n = 3$ per group. **e** Representative western blots for FOXO3a and GAPDH in testes of different mice. Right: quantitative analysis of the FOXO3a protein level, relative to GAPDH. $n = 3$ per group. **f** Left: representative images of testicular sections from indicated groups. The sections were stained with LCs marker CYP17A1, and SA-β-gal. Scale bar: 75 μm. Right: quantitative analysis of the CYP17A1$^+$ SA-β-gal$^+$ cells. $n = 3$ per group. **g** Left: representative confocal images of testicular sections from indicated groups. The sections were stained with senescence marker p21, HSD3β, and DAPI. Scale bar: 50 μm. Right: quantitative analysis of the p21$^+$ HSD3β$^+$ cells. $n = 3$ per group. **h, i** Quantitative RT-PCR analysis of senescence markers (*p21*, *Cxcl10*). $n = 3$ per group. **j**–**m** Serum testosterone (**j**), intratesticular testosterone (**k**), serum Insl3 (**l**), serum LH (**m**) level of the indicated groups. $n = 20$ per group in (**j**), $n = 5$ per group in (**k**), $n = 12$ per group in (**l**), $n = 12$ per group in (**m**). **n**–**q** Representative light micrographs of sperm acquired from indicated groups (**n**). Scale bar: 100 μm. Sperm concentration (**o**), proportion of sperm with motility (**p**), proportion of sperm with progressive motility (**q**). $n = 10$ per group. Data were presented as mean ± SEM. Significance was determined by one-way ANOVA (**b-water consumed, c–h, k, o–q**) or Kruskal-Wallis test (**b-food consumed, i, j, l, m**). Illustrations were created with BioRender. Source data are provided as a Source Data file.

from GemPharmatech (Foshan, Guangdong, China). The *Hmgcs2*^{flox} mouse line was generated using CRISPR/Cas9 technology by GemPharmatech (Nanjing, Jiangsu, China). Male mice were identified by PCR performed on DNA isolated from tail samples. All mice were housed in the Sun Yat-sen University Animal Center under specific conditions of constant temperature (24 ± 1 °C), relative humidity (50–60%), and a 12 h light/12 h dark cycle. They were provided ad libitum access to food and water throughout the study. The diet was purchased from Xietong Pharmaceutical Bio-Engineering Co.,Ltd. (Jiangsu, CAT# XT-SL-2KG). The animal use protocol has been reviewed and approved by the Institutional Animal Care and Use Committee (IACUC), Sun Yat-Sen University (Approval No. SYSU-IACUC-2022-001335). Strict adherence to animal welfare and ethical considerations was ensured throughout the study. The primers for genotyping are listed in the Supplementary Table 1.

Sample Preparation for Single-Cell RNA Sequencing

2-month-old and 24-month-old mice were anesthetized with Avertin (250 mg/kg) by i.p. injection. After dissection, the testes were immediately placed in ice-cold saline. After fully washing the testes with phosphate-buffered saline (PBS), the tunica albuginea was carefully removed. The testes were mechanically minced into pieces using microscopic forceps and digested with accutase (Invitrogen, USA) at 37 °C for 5 minutes. The accutase activity was halted by adding DMEM/F12 supplemented with 10% fetal bovine serum (Gibco, USA), and the samples were rinsed twice with PBS. The obtained cell suspension was filtered through a 45 μm strainer and centrifuged. At last, cells were resuspended in PBS containing 0.1% BSA (Thermo Fisher Scientific, USA) at a concentration of ~1000 cells/μL for single-cell sequencing.

Single Cell RNA-seq Performance, Library Preparation and Sequencing

The BD Rhapsody system was used to capture the transcriptomic information. Single-cell capture was achieved by randomly distributing a single-cell suspension across microwells using a limited dilution approach. Beads with oligonucleotide barcodes were added in excess to ensure that a bead paired with a cell in each microwell. Cell-lysis buffer was added to allow poly-adenylated RNA molecules to hybridize to the beads. The beads were collected into a single tube for reverse transcription. Whole transcriptome libraries were prepared using the BD Rhapsody single-cell whole-transcriptome amplification workflow. Sequencing libraries were quantified using a High Sensitivity DNA chip (Agilent, USA) on a Bioanalyzer 2200 and the Qubit High Sensitivity DNA assay (Thermo Fisher Scientific, USA). The library for each sample was sequenced using an Illumina sequencer (Illumina, CA).

Single Cell RNA Sequencing quality control

The Seurat package (version 4.3.1)[66] was utilized for basic data processing. Briefly, cells that met the following criteria were retained: (1) total number of expressed genes (nFeature RNA) between 300 and 8000; (2) total unique molecular identifier (UMI) count (nCount RNA) < 60,000; and (3) mitochondrial gene percentage (Percent.mt) <50%. Cells not meeting these thresholds were excluded from analysis to reduce potential technical noise and improve the quality of the dataset. Then the data were log-normalized and scaled. Variable genes were identified by the 'FindVariableGenes' function. Next, principal component analysis (PCA) was performed, and the top 30 principal components (PCs) were used for t-distributed stochastic neighbor embedding (tSNE) dimension reduction and clustering. The DoubletFinder package (version 2.0.4) was employed to calculate and remove doublets. Then the data were pre-processed again and used for subsequent analyses.

Cell-type identification

After quality control, canonical correlation analysis (CCA) was employed for data integration and to remove batch effects. Cells were visualized using tSNE algorithm. Cell types were identified based on the indicated marker genes (refer to the Results section). Marker genes for each cluster were determined using the 'FindAllMarkers' function with the Wilcoxon rank-sum test. Only genes with |avg_logFC| > 0.4, min.pct > 0.5, and an adjusted P value < 0.05 were considered as marker genes. Gene enrichment analysis of cell type-specific markers, based on the Gene Ontology (GO) database, was conducted using clusterProfiler (Version 4.8.3)[67].

Pseudotime analysis

The Seurat object of LCs was converted to a CellDataSet object to facilitate import into the monocle package (v2.28.0). Pseudotime analysis was performed using the default settings. Aging-associated DEGs of LCs were identified using the 'FindMarkers' function with default settings. LCs were arranged according to pseudotime and visualized using the pheatmap package (version 1.0.12).

Gene set enrichment analysis

Gene Set Enrichment Analysis (GSEA) on Gene Ontology (GO) terms was performed using the 'gseGO' function in the clusterProfiler R package (v4.8.3). Enrichment was considered significant for terms with adjusted P value < 0.05 and |Normalized Enrichment Score (NES)| > 1. The results were visualized using ggplot2 (version 3.5.0).

Bulk RNA-seq

Raw RNA sequencing data from vehicle- or Hymeglusin-treated MLTC-1 cells were pre-processed using fastp (version 0.23.4) and FastQC (version 0.12.1). Paired-end clean reads were mapped to the mm10 mouse reference genome using HISAT2 (version 2.2.1). Gene expression profiles were quantified using featureCounts (version 2.0.6) to obtain read counts for subsequent analysis. Differential gene expression between groups was analyzed using the DESeq2 package (version 1.40.2). Differentially expressed genes (DEGs) were selected based on a |log2(Fold Change)| > 1 and an adjusted P value < 0.05 for statistical significance.

Ketone bodies measurement

The concentration of BHB in the blood was quantitatively measured using a blood ketone meter (Abbott, USA). Blood samples were collected from the tail vein of mice using standard procedures. A small incision was made using a sterile scalpel and the tip of the strip was then brought into contact with a blood droplet from the tail vein. The strip drew the whole blood into the blood channel via capillary action. The meter began measuring the BHB concentration once the channel was completely filled.

To detect the concentration of AcAc in the blood, samples were collected from the mandibular vein of the mice and left to clot for 1 hour. The samples were then centrifuged at 5000 g for 10 minutes, and the supernatant serum was collected for subsequent analyses. Supernatants were tested according to the protocol provided by the colorimetric kit (Abcam, USA) manufacturer.

To detect the concentrations of ketone bodies in the testes, colorimetric kits were used to analyze AcAc (Abcam, USA) and BHB (Cayman, USA). Testes were collected and placed in 1 ml of saline with two 4 mm beads (Easybio, China). The tissues were homogenized using a high-throughput tissue lyser at a frequency of 50 Hz for 5 minutes. The homogenate was then centrifuged at 10000 g for 3 minutes, and 100 μl of the supernatant was collected and diluted tenfold with saline. The concentrations of ketone bodies were detected according to the manufacturer's instructions.

To detect intracellular ketone bodies concentrations, colorimetric kits were used to analyze AcAc (Abcam, USA) and BHB (Cayman,

USA). The cell culture medium was discarded, the cells were washed three times with saline, and then 1 ml of 80% methanol solution (pre-cooled at −20 °C for 6 hours) was added. After lysis, a cell scraper (NEST, China) was used to transfer the mixture to a 1.5 ml centrifuge tube. The mixture was vortexed for 5 minutes, then centrifuged at 13,000 g for 10 minutes at 4 °C, and the supernatant was collected for subsequent detection. Supernatants were tested according to the protocol provided by the colorimetric kit manufacturer.

Isolation of LCs

Isolation of LCs from wild-type mice was performed as previously described by our group[68]. In brief, the tunica albuginea was carefully removed, and the testes were mechanically minced and enzymatically dissociated using 200 μg/mL DNase I (Gibco, USA) and 1 mg/mL Type IV Collagenase (Gibco, USA) in Dulbecco's Modified Eagle Medium/Nutrient Mixture F-12 (DMEM/F12; 1:1, Gibco, USA) at 37 °C for 15 minutes with gentle agitation (100 cycles/min). The collagenase activity was halted by adding DMEM/F12 supplemented with 10% fetal bovine serum (Gibco, USA), and the samples were rinsed twice with PBS. The resulting cell suspension was filtered through a 45 μm strainer to obtain a single-cell suspension. LCs were subsequently sorted using flow cytometry (Beckman Coulter, USA). For isolation of LCs from AAV-infected testes, the single-cell suspension was prepared according to the above method. GFP^+ or $mCherry^+$ LCs were subsequently sorted using flow cytometry (Beckman Coulter, USA).

Production of lentivirus

HEK293T cells were cultured in DMEM (Corning, USA) supplemented with 10% FBS, 1% Penicillin-Streptomycin (Gibco, USA), and 1% GlutaMAX (Gibco, USA). To package lentivirus for the construction of a HEK-293 reporter cell line, HEK293T cells were seeded in a T75 flask (NEST, China). When cells reached 90% confluency, a mixture of 4.5 μg of lentiviral transfer plasmid, 3 μg of psPAX, and 1.5 μg of pMD2.G was co-transfected using Lipo8000™ Transfection Reagent (Beyotime, China). Twelve hours after transfection, the media was replaced. At 48 and 72 hours post-transfection, the supernatant was collected and then filtered through a 0.45 μm sterile filter (Millipore, USA). Subsequently, the lentivirus was centrifuged at 50,000 g for 90 minutes, resuspended in 0.5 mL PBS, and stored at −80 °C.

Construction of gene knockdown cell line

MLTC-1 cells were cultured in RPMI 1640 (Corning, USA) supplemented with 10% FBS (Gibco, USA), 1% Penicillin-Streptomycin (Gibco, USA), and 1% GlutaMAX (Gibco, USA). Sh-RNA sequences (Supplementary Table 2) were cloned into pLKO.1-copGFP-PURO plasmids by Singke Biotech. The plasmids were used for the production of lentiviral vectors. At 70% confluence, the cells were transfected with lentivirus containing shRNA sequences in the presence of 8 μg/mL polybrene. Four days post-transduction, the cells were digested with 0.25% trypsin at 37 °C for 3 minutes and then filtered through a 45 μm strainer to obtain a single-cell suspension. GFP^+ cells were subsequently sorted using flow cytometry (Beckman Coulter, USA) for further experiments.

RNA extraction, cDNA synthesis, and quantitative RT-PCR

Total RNA was extracted from testes or cells using the RNeasy Mini Kit (Yibin, China) according to the manufacturer's protocol. RNA purity was assessed by measuring the 260/280 ratio (1.87–1.93) and the 260/230 ratio (2.18–2.34) using a NanoDrop 1000 spectrophotometer (Thermo Fisher Scientific, USA). Reverse transcription was performed using the NovoScript® 1st Strand cDNA Synthesis Kit (Novoprotein, China). Quantitative RT-PCR was carried out using SYBR PCR Master Mix (Roche, CH) and a LightCycler 480 Detection System (Roche, CH). Primer validation was performed by generating a melting curve to confirm a single peak, thereby ruling out the possibility of non-specific product or primer dimer formation. β-actin served as an internal control, and target gene expression levels were calculated using the ΔCt method and expressed relative to β-actin. The primers are listed in the Supplementary Table 3.

Induce cell premature senescence and treatment with AcAc or BHB

To induce premature senescence, H_2O_2 (Hengjian, China) was added to the medium at a concentration of 100 μM. After 24 hours of exposure to H_2O_2, BHB or AcAc was added to the culture medium. All groups were analyzed on the fourth day. Doxorubicin (MCE, USA) was dissolved in DMSO, stored at −20 °C, and then added to the culture medium at a concentration of 150 nM with a 24-hour interval between treatments. 24 hours after adding doxorubicin, BHB or AcAc was added to the culture medium. All groups were analyzed on the fifth day. For inducing premature senescence by radiation, cells were exposed to 8 Gy of ionizing radiation using an RS 2000 X-ray Biological Irradiator (Rad Source, USA) at a dose rate of 1.185 Gy/min. 3 days post-irradiation, BHB or AcAc was added to the culture medium. Subsequently, the cells were cultured under standard conditions. 3-Hydroxybutyric acid sodium (MCE, USA) and Lithium acetoacetate (Sigma, USA) were both dissolved in saline, stored at −80 °C, and added to the culture medium at a concentration of 5 mM.

ChIP-qPCR

A ChIP assay kit (CST, USA) was employed to assess the binding of H3K9ac to the promoters of *Foxo3a*. MLTC-1 cells were seeded in a T75 flask (NEST, China). Following treatment, cells at 70% confluence were fixed with 1% formaldehyde on ice to cross-link proteins to chromatin DNA. After washing, the chromatin DNA was enzymatically sheared to produce DNA fragments ranging from 200 to 1,000 bp. Subsequently, DNA recovery was performed according to the manufacturer's protocol. The recovered DNA from the reverse cross-linking was utilized for qPCR analysis. An equal amount of sheared DNA without antibody precipitation was processed for reverse cross-linking and utilized as an input control. The primers are listed in the Supplementary Table 4.

Western blot

For protein extraction from cultured cells, cells were washed three times with ice-cold PBS. Subsequently, the cells were lysed directly in RIPA buffer (Beyotime, China) for 30 min, followed by centrifugation at 13000 g for 10 min at 4 °C. Each supernatant was recovered as a total cell lysate. For protein extraction from tissue, testes were grinded in liquid nitrogen and subsequently lysed with RIPA Buffer (Beyotime, China). The lysates were placed on ice for 30 minutes and then centrifuged at 12,000 g for 15 minutes at 4 °C. Supernatants containing proteins were collected, and protein concentrations were determined using Pierce™ BCA Protein Assay Kits (Thermo Fisher, USA). The lysates were resolved by SDS polyacrylamide gel electrophoresis and then transferred onto 0.45 μm pore-sized polyvinylidene fluoride membranes (Millipore, USA). Subsequently, the membranes were blocked with 5% milk (Phygene, China), incubated with primary antibodies overnight at 4 °C, washed with tris-buffered saline Tween-20 (TBST), and incubated with HRP-conjugated secondary antibodies for 1 hour at room temperature. Finally, the signals were visualized using an ECL substrate (NCM, China). Immunoreactivity was semi-quantitatively detected by ChemiDoc Imaging Systems (Bio-Rad, USA). The primary and secondary antibodies are listed in the Supplementary Table 5.

Immunofluorescence staining

For immunofluorescence staining of sections, the tissues were fixed in 4% paraformaldehyde (PFA; Phygene, China) at 4 °C for 4 hours, dehydrated with 30% sucrose (Sangon Biotech, China),

and sectioned at a thickness of 10 μm. The sections underwent antigen retrieval using Citrate Antigen Retrieval Solution (Beyotime, China), followed by permeabilization with 0.2% Triton X-100 (Sigma, USA) for 15 minutes. After blocking with 2% BSA (Sigma, USA) and 10% goat serum (Boster, China) in PBS for 45 minutes at room temperature, sections were incubated overnight with primary antibodies. Subsequently, sections were washed with PBS five times, incubated with appropriate secondary antibodies for 60 minutes at room temperature, and counterstained with DAPI (Gibco) for 5 minutes. Images were captured using an LSM800 confocal microscope (Zeiss, Germany) or a Nikon C2 confocal microscope (Nikon, Japan). For immunofluorescence staining of cells, the cells were seeded in a 24-well plate and fixed in 4% PFA (Phygene, China) for 15 minutes. Fixed cells were permeabilized with PBS containing 0.2% Triton X-100 for 15 minutes at room temperature. Non-specific antibody binding was blocked with 2% BSA and 10% goat serum in PBS for 45 minutes at room temperature, followed by overnight incubation with relevant primary antibodies at 4 °C. Next, cells were washed three times with PBS and incubated with appropriate secondary antibodies for 45 minutes at room temperature. Finally, the nuclei were counterstained with DAPI for 5 minutes, and images were captured using an LSM800 confocal microscope (Zeiss, Germany) or a Nikon C2 confocal microscope (Nikon, Japan). The primary and secondary antibodies are listed in the Supplementary Table 6.

H&E staining

The testes were collected, fixed overnight in Bouin's solution (Sigma, USA), dehydrated in 75% ethanol, embedded in paraffin, and then sectioned into 4 μm-thick slices. Subsequently, the paraffin-embedded sections were deparaffinized using xylene and then gradually rehydrated with a series of ethanol concentrations. For histological analysis, the prepared sections were stained with haematoxylin and eosin (H&E). The stained sections were examined using KF-PRO-120-H1 slide scanner (KFBIO, China).

SA-β-gal staining

According to the manufacturer's protocol for the senescence-associated β-galactosidase kit (Beyotime, China), cells seeded in 12-well plates were washed with PBS and subsequently fixed in β-galactosidase staining fixative (Beyotime, China) for 15 minutes. After washing, the cells were incubated overnight with the working solution at 37 °C. Senescent cells were observed and counted under an DMi8 microscope (Leica, Germany) from three random fields of view. For SA-β-gal staining of tissue sections, the O.C.T (optimal cutting temperature compound)-embedded testicular tissues were cryosectioned at a thickness of 10 μm, and stored at −80 °C. Before SA-β-Gal staining, sections were thawed at RT and rinsed in PBS for 1 min, fixed in in β-galactosidase staining fixative (Beyotime, China) at RT for 15 min. The sections were then stained according to the manufacturer's protocol for 6 hours. After staining, the sections were retrieved using Citrate Antigen Retrieval Solution (Beyotime, China), permeabilized with 0.2% Triton X-100 (Sigma, USA) for 15 minutes, blocked with 2% BSA (Sigma, USA) and 10% goat serum (Boster, China) in PBS for 45 minutes at room temperature, and then subsequently incubated overnight with primary antibodies. Following incubation, the sections were washed five times with PBS, incubated with appropriate secondary antibodies for 60 minutes at room temperature, and images were captured using DMi8 microscope (Leica, Germany).

Computer-aided semen analysis

Semen samples were analysed as previously reported[30]. In brief, two cauda epididymides were harvested from each mouse, incised with micro scissors, and then incubated in 1 mL DMEM/F12 containing 0.5% BSA for 15 min at 37 °C to allow for sperm release. The tissue was removed, and sperm samples were analysed using a Hamilton Thorne's Ceros II system. At least six fields were assessed for each sample, and the sperm concentration and percentages of motile and progressively motile spermatozoa were determined.

Sex hormone assays

Sex hormone concentrations were assayed as previously reported by our group[69]. In brief, blood was collected from the mandibular vein of the mice and left to clot for 1 hour. The samples were then centrifuged at 5000 g for 10 minutes, and the supernatant serum was collected for subsequent analyses. For intratesticular testosterone concentration detection, testes were extracted from the mice and placed in 1 ml of saline with two 4 mm beads (Easybio, China). A high-throughput tissue crusher was used to crush the testicular tissue at a frequency of 50 Hz for 5 minutes. Subsequently, the sample was centrifuged at 10,000 g for 3 minutes, and 100 μl of the supernatant was collected and diluted tenfold with physiological saline. Serum and testes samples were collected at the indicated time points and stored at −80 °C until analysis. Testosterone levels were measured using a chemiluminescent immunoassay (CLIA) (KingMed Diagnostics Group Co, Ltd, China). The minimum detectable dose of testosterone is 0.01 ng/mL. The concentration of serum LH and FSH was calculated based on the instructions provided by the manufacturer using an Elisa kit (Cloud-clone, China). The concentration of serum Insl3 was calculated based on the instructions provided by the manufacturer using an Elisa kit (Phoenix, USA). To detect the ability of cells to secrete progesterone, MLTC-1 cells were washed three times with PBS, and then fresh RPMI 1640 medium containing 10% FBS and 1% GlutaMAX was added. After 4 hours, the culture supernatant was collected for subsequent detection, and the cells were digested with 0.25% trypsin for cell counting using a computer-assisted system (Nexcelom, USA).

Gene delivery in animal models

For *Hmgcs2* overexpression, the full-length mouse *Hmgcs2* cDNA was cloned into the AAV-CAG vector. Wild-type aged mice (15-month-old) were intratesticularly injected with AAVDJ-*Hmgcs2* for *Hmgcs2* overexpression. For conditional knockout (CKO), the full-length Cre cDNA was inserted into the AAV-CAG vector. Eight-week-old male *Hmgcs2*$^{fl/fl}$ mice were intratesticularly injected with AAVDJ-Cre for conditional knockout. Following sequencing-based verification, the constructed vector was custom-packaged, purified, and titrated by Packgene Bioscience (Guangzhou, China). The viruses were stored at −80 °C until use. For gene delivery, mice were anesthetized with Avertin (250 mg/kg) via intraperitoneal injection. The injection site was sterilized with ethanol and a topical application of povidone-iodine. The mice testes were stabilized through the scrotum with fingers, and AAV particles were injected into the testes using an insulin syringe (20 μL per testis; 2×10^9 genome copies per testis). After injection, the needle was retained inside the tissue for 30 seconds to allow the virus to disperse within the testis.

BHB supplementation in aged mice

Wild-type aged mice (18-months-old) received sodium/potassium salt supplementation in their drinking water. The KetoForce solution is a BHB salt with 1.6 g of sodium and potassium per 11.7 g of BHB. 10 ml BHB salt formulation (KetoForce) was administered in 290 ml of drinking water for BHB supplementation. For the control group, 3.2 g of sodium chloride and 2.4 g of potassium chloride were added to 250 ml of water. Both the experimental group and the control group were supplemented with equivalent sodium and potassium.

Statistical analysis

All data were subjected to statistical analysis using IBM SPSS Statistics version 25.0 software (IBM SPSS Statistics, Armonk, NY, USA) and the results were visualized using GraphPad Prism 9 software (GraphPad

Software, La Jolla, CA, USA). The bioinformatics data were analyzed using R (version 4.0.3). Gene Ontology (GO) enrichment analysis was assessed using a one-sided hypergeometric test with Benjamini-Hochberg (BH) correction. Gene Set Enrichment Analysis (GSEA) was performed using a two-sided permutation test with BH correction. Differentially expressed genes (DEGs) between Leydig cells (LCs) from young and old groups were identified using a two-sided Wilcoxon rank-sum test with Bonferroni correction. For experiments excluding RNA-seq data, statistical differences between samples were assessed with t-tests, one-way analysis of variance (ANOVA), Mann-Whitney U test, or Kruskal-Wallis test. Differences were considered significant when $p < 0.05$, and p values were indicated in figures. The detailed statistical analyses have been provided in the Source Data file.

Reporting summary

Further information on research design is available in the Nature Portfolio Reporting Summary linked to this article.

Data availability

The scRNA-seq data generated in this study have been deposited in the GEO database under accession code GSE270931. The bulk RNA-seq data generated in this study have been deposited in the GEO database under accession code GSE287203. The rest of the data generated in this study are included in the published article and supplementary files. Source data are provided with this paper.

References

1. Finkelstein, J. S. et al. Gonadal steroids and body composition, strength, and sexual function in men. *N. Engl. J. Med* **369**, 1011–1022 (2013).
2. Oatley, J. M. & Brinster, R. L. The germline stem cell niche unit in mammalian testes. *Physiol. Rev.* **92**, 577–595 (2012).
3. Basaria, S. Reproductive aging in men. *Endocrinol. Metab. Clin. North Am.* **42**, 255–270 (2013).
4. Paul, C. & Robaire, B. Ageing of the male germ line. *Nat. Rev. Urol.* **10**, 227–234 (2013).
5. Juul, A. & Skakkebaek, N. E. Androgens and the ageing male. *Hum. Reprod. Update* **8**, 423–433 (2002).
6. Ramasamy, R., Wilken, N., Scovell, J. M. & Lipshultz, L. I. Effect of testosterone supplementation on symptoms in men with hypogonadism. *Eur. Urol.* **67**, 176–177 (2015).
7. Bhasin, S. et al. Testosterone Therapy in Men With Hypogonadism: An Endocrine Society Clinical Practice Guideline. *J. Clin. Endocrinol. Metab.* **103**, 1715–1744 (2018).
8. Cappola, A. R. Testosterone therapy and risk of cardiovascular disease in men. *JAMA* **310**, 1805–1806 (2013).
9. Halpern, J. A. & Brannigan, R. E. Testosterone Deficiency. *JAMA* **322**, 1116 (2019).
10. Bremner, W. J. Testosterone deficiency and replacement in older men. *N. Engl. J. Med* **363**, 189–191 (2010).
11. Suryadevara, V. et al. SenNet recommendations for detecting senescent cells in different tissues. *Nat. Rev. Mol. Cell Biol.* **25**, 1001–1023 (2024).
12. Lopez-Otin, C., Blasco, M. A., Partridge, L., Serrano, M. & Kroemer, G. Hallmarks of aging: An expanding universe. *Cell* **186**, 243–278 (2023).
13. van Deursen, J. M. The role of senescent cells in ageing. *Nature* **509**, 439–446 (2014).
14. Xu, M. et al. Transplanted Senescent Cells Induce an Osteoarthritis-Like Condition in Mice. *J. Gerontol. A Biol. Sci. Med Sci.* **72**, 780–785 (2017).
15. Xu, M. et al. Senolytics improve physical function and increase lifespan in old age. *Nat. Med* **24**, 1246–1256 (2018).
16. Palla, A. R. et al. Inhibition of prostaglandin-degrading enzyme 15-PGDH rejuvenates aged muscle mass and strength. *Science*. https://doi.org/10.1126/science.abc8059 (2021).
17. Niu, F. et al. Aberrant hyper-expression of the RNA binding protein GIGYF2 in endothelial cells modulates vascular aging and function. *Redox Biol.* **65**, 102824 (2023).
18. Perheentupa, A. & Huhtaniemi, I. Aging of the human ovary and testis. *Mol. Cell Endocrinol.* **299**, 2–13 (2009).
19. Kaufman, J. M., Lapauw, B., Mahmoud, A., T'Sjoen, G. & Huhtaniemi, I. T. Aging and the Male Reproductive System. *Endocr. Rev.* **40**, 906–972 (2019).
20. Johnson, L., Nguyen, H. B., Petty, C. S. & Neaves, W. B. Quantification of human spermatogenesis: germ cell degeneration during spermatocytogenesis and meiosis in testes from younger and older adult men. *Biol. Reprod.* **37**, 739–747 (1987).
21. Lipsett, M. B. Physiology and pathology of the Leydig cell. *N. Engl. J. Med* **303**, 682–688 (1980).
22. Lee, S. Y. et al. ROS inhibit the expression of testicular steroidogenic enzyme genes via the suppression of Nur77 transactivation. *Free Radic. Biol. Med* **47**, 1591–1600 (2009).
23. Alfano, M. et al. Aging, inflammation and DNA damage in the somatic testicular niche with idiopathic germ cell aplasia. *Nat. Commun.* **12**, 5205 (2021).
24. Huang, D. et al. A single-nucleus transcriptomic atlas of primate testicular aging reveals exhaustion of the spermatogonial stem cell reservoir and loss of Sertoli cell homeostasis. *Protein Cell* **14**, 888–907 (2023).
25. Deng, Z. et al. Targeting dysregulated phago-/auto-lysosomes in Sertoli cells to ameliorate late-onset hypogonadism. *Nat. Aging* **4**, 647–663 (2024).
26. He, S. & Sharpless, N. E. Senescence in Health and Disease. *Cell* **169**, 1000–1011 (2017).
27. Cheng, C. W. et al. Ketone Body Signaling Mediates Intestinal Stem Cell Homeostasis and Adaptation to Diet. *Cell* **178**, 1115–1131 e1115 (2019).
28. Puchalska, P. & Crawford, P. A. Multi-dimensional Roles of Ketone Bodies in Fuel Metabolism, Signaling, and Therapeutics. *Cell Metab.* **25**, 262–284 (2017).
29. Darbey, A. et al. A comparison of in vivo viral targeting systems identifies adeno-associated virus serotype 9 (AAV9) as an effective vector for genetic manipulation of Leydig cells in adult mice. *Andrology* **9**, 460–473 (2021).
30. Zhang, S. et al. AAV-mediated gene therapy restores natural fertility and improves physical function in the Lhcgr-deficient mouse model of Leydig cell failure. *Cell Prolif.* **57**, e13680 (2024).
31. Gorgoulis, V. et al. Cellular Senescence: Defining a Path Forward. *Cell* **179**, 813–827 (2019).
32. Zhang, C. et al. FOXO4-DRI alleviates age-related testosterone secretion insufficiency by targeting senescent Leydig cells in aged mice. *Aging (Albany NY)* **12**, 1272–1284 (2020).
33. Sun, T. et al. Characterization of cellular senescence in doxorubicin-induced aging mice. *Exp. Gerontol.* **163**, 111800 (2022).
34. Yang, D. et al. NKG2D-CAR T cells eliminate senescent cells in aged mice and nonhuman primates. *Sci. Transl. Med* **15**, eadd1951 (2023).
35. Xie, Z. et al. Metabolic Regulation of Gene Expression by Histone Lysine beta-Hydroxybutyrylation. *Mol. Cell* **62**, 194–206 (2016).
36. Shimazu, T. et al. Suppression of oxidative stress by beta-hydroxybutyrate, an endogenous histone deacetylase inhibitor. *Science* **339**, 211–214 (2013).
37. Benjamin, D. I. et al. Fasting induces a highly resilient deep quiescent state in muscle stem cells via ketone body signaling. *Cell Metab.* **34**, 902–918 e906 (2022).
38. Yan, P. et al. FOXO3-Engineered Human ESC-Derived Vascular Cells Promote Vascular Protection and Regeneration. *Cell Stem Cell* **24**, 447–461 e448 (2019).
39. Tsai, W. B., Chung, Y. M., Takahashi, Y., Xu, Z. & Hu, M. C. Functional interaction between FOXO3a and ATM regulates DNA damage response. *Nat. Cell Biol.* **10**, 460–467 (2008).

40. Ohzono, H. et al. Targeting FoxO transcription factors with HDAC inhibitors for the treatment of osteoarthritis. *Ann. Rheum. Dis.* **82**, 262–271 (2023).
41. Xia, K. et al. Single-cell RNA sequencing reveals transcriptomic landscape and potential targets for human testicular ageing. *Hum. Reprod.* **39**, 2189–2209 (2024).
42. Santiago, J., Silva, J. V., Alves, M. G., Oliveira, P. F. & Fardilha, M. Testicular Aging: An Overview of Ultrastructural, Cellular, and Molecular Alterations. *J. Gerontol. A Biol. Sci. Med Sci.* **74**, 860–871 (2019).
43. Zirkin, B. R. & Papadopoulos, V. Leydig cells: formation, function, and regulation. *Biol. Reprod.* **99**, 101–111 (2018).
44. Mendonca, B. B., Costa, E. M., Belgorosky, A., Rivarola, M. A. & Domenice, S. 46,XY DSD due to impaired androgen production. *Best. Pr. Res Clin. Endocrinol. Metab.* **24**, 243–262 (2010).
45. Teerds, K. J. & Huhtaniemi, I. T. Morphological and functional maturation of Leydig cells: from rodent models to primates. *Hum. Reprod. Update* **21**, 310–328 (2015).
46. Di Micco, R., Krizhanovsky, V., Baker, D. & d'Adda di Fagagna, F. Cellular senescence in ageing: from mechanisms to therapeutic opportunities. *Nat. Rev. Mol. Cell Biol.* **22**, 75–95 (2021).
47. Hanukoglu, I. Antioxidant protective mechanisms against reactive oxygen species (ROS) generated by mitochondrial P450 systems in steroidogenic cells. *Drug Metab. Rev.* **38**, 171–196 (2006).
48. Robinson, A. M. & Williamson, D. H. Physiological roles of ketone bodies as substrates and signals in mammalian tissues. *Physiol. Rev.* **60**, 143–187 (1980).
49. Matsuura, T. R., Puchalska, P., Crawford, P. A. & Kelly, D. P. Ketones and the Heart: Metabolic Principles and Therapeutic Implications. *Circ. Res* **132**, 882–898 (2023).
50. Lin, Y. H. et al. Ketone bodies promote stroke recovery via GAT-1-dependent cortical network remodeling. *Cell Rep.* **42**, 112294 (2023).
51. Tomita, I. et al. SGLT2 Inhibition Mediates Protection from Diabetic Kidney Disease by Promoting Ketone Body-Induced mTORC1 Inhibition. *Cell Metab.* **32**, 404–419 e406 (2020).
52. Puchalska, P. et al. Hepatocyte-Macrophage Acetoacetate Shuttle Protects against Tissue Fibrosis. *Cell Metab.* **29**, 383–398 e387 (2019).
53. Zou, X. et al. Acetoacetate Accelerates Muscle Regeneration and Ameliorates Muscular Dystrophy in Mice. *J. Biol. Chem.* **291**, 2181–2195 (2016).
54. Kops, G. J. et al. Forkhead transcription factor FOXO3a protects quiescent cells from oxidative stress. *Nature* **419**, 316–321 (2002).
55. Chung, W. H., Dao, R. L., Chen, L. K. & Hung, S. I. The role of genetic variants in human longevity. *Ageing Res Rev.* **9**, S67–S78 (2010).
56. Zhang, W. et al. A single-cell transcriptomic landscape of primate arterial aging. *Nat. Commun.* **11**, 2202 (2020).
57. Huffman, J. & Kossoff, E. H. State of the ketogenic diet(s) in epilepsy. *Curr. Neurol. Neurosci. Rep.* **6**, 332–340 (2006).
58. Veech, R. L., Chance, B., Kashiwaya, Y., Lardy, H. A. & Cahill, G. F. Jr. Ketone bodies, potential therapeutic uses. *IUBMB Life* **51**, 241–247 (2001).
59. Xie, S. et al. Dietary ketone body-escalated histone acetylation in megakaryocytes alleviates chemotherapy-induced thrombocytopenia. *Sci. Transl. Med* **14**, eabn9061 (2022).
60. Monda, A. et al. Exploring the ketogenic diet's potential in reducing neuroinflammation and modulating immune responses. *Front Immunol.* **15**, 1425816 (2024).
61. Menyhart, O. & Gyorffy, B. Dietary approaches for exploiting metabolic vulnerabilities in cancer. *Biochim Biophys. Acta Rev. Cancer* **1879**, 189062 (2024).
62. Zhu, D. et al. Intrapericardial Exosome Therapy Dampens Cardiac Injury via Activating Foxo3. *Circ. Res* **131**, e135–e150 (2022).
63. Xiao, Y. et al. Comparative single-cell transcriptomic analysis across tissues of aging primates reveals specific autologous activation of ZNF281 to mitigate oxidative stress in cornea. *Aging Cell* **23**, e14319 (2024).
64. White, R. R. et al. FOXO3a acts to suppress DNA double-strand break-induced mutations. *Aging Cell* **19**, e13184 (2020).
65. Webb, A. E., Kundaje, A. & Brunet, A. Characterization of the direct targets of FOXO transcription factors throughout evolution. *Aging Cell* **15**, 673–685 (2016).
66. Hao, Y. et al. Integrated analysis of multimodal single-cell data. *Cell* **184**, 3573–3587 e3529 (2021).
67. Yu, G., Wang, L. G., Han, Y. & He, Q. Y. clusterProfiler: an R package for comparing biological themes among gene clusters. *OMICS* **16**, 284–287 (2012).
68. Luo, P. et al. An autofluorescence-based isolation of Leydig cells for testosterone deficiency treatment. *Mol. Cell Endocrinol.* **535**, 111389 (2021).
69. Xia, K. et al. Precise Correction of Lhcgr Mutation in Stem Leydig Cells by Prime Editing Rescues Hereditary Primary Hypogonadism in Mice. *Adv. Sci. (Weinh.)* **10**, e2300993 (2023).

Acknowledgements

This work was supported by National Key Research and Development Program of China(2022YFA1104100 to A.P.X.), National Natural Science Foundation of China (82430050 to A.P.X., 32130046 to A.P.X., 82371611 to K.X., 82371609 to C.D., 82171564 to P.L., 82101669 to K.X., 82301847 to H.C., 82171617 to Q.K., 82301796 to P.L.), Key Research and Development Program of Guangdong Province (2019B020235002 to Q.K.), Natural Science Foundation of Guangdong Province (2022A1515010371 to K.X.), Key Scientific and Technological Program of Guangzhou City (2023B01J1002 to A.P.X.), Pioneering talents project of Guangzhou Development Zone (2021-L029 to A.P.X.), Shenzhen Nanshan District Health System Science and Technology Major Project (NSZD2023049 to H.C.), Sanming Project of Medicine in Shenzhen Nanshan (SZSM202103012 to A.P.X.). Figures 1a, 2c, 3a, 4a, 5a, 6a, 7a and Supplementary Fig. 6d, h were created using BioRender (https://app.biorender.com/).

Author contributions

C.L., H.P., J.Y. and P.L. carried out the experiments and data analysis, design the experimental, and wrote the manuscript. J.Y. and Y.M. analyzed scRNA-seq data. P.L. and H.C. assisted with the animal experiments. S.Z. and H.P. helped with immunofluorescence staining. W.O., C.X., C.Y., L.Z., H.F., X.G. and Y.Z. assisted with animal experiments and genotyping. T.W., Q.K., W.L. and C.D. assisted with the experimental design and revised the manuscript. A.P.X. and K.X. conceived the project, supervised all experiments, and revised the manuscript. All authors fulfill the criteria for authorship.

Competing interests

The authors declare no competing interests.

Additional information

Supplementary information The online version contains supplementary material available at https://doi.org/10.1038/s41467-025-59591-8.

Correspondence and requests for materials should be addressed to Andy Peng Xiang or Kai Xia.

Peer review information *Nature Communications* thanks Ana Gomes and the other anonymous reviewer(s) for their contribution to the peer review of this work. A peer review file is available.